*Journal of The Electrochemical Society*, **158** (12) A1461-A1477 (2011)
0013-4651/2011/158(12)/A1461/17/$28.00 © The Electrochemical Society


# Coordinate Transformation, Orthogonal Collocation, Model Reformulation and Simulation of Electrochemical-Thermal Behavior of Lithium-Ion Battery Stacks

**Paul W. C. Northrop,* Venkatasailanathan Ramadesigan,* Sumitava De,* and Venkat R. Subramanian**,z**

*Department of Energy, Environmental and Chemical Engineering, Washington University, Saint Louis, Missouri 63130, USA*

In this paper, a simple transformation of coordinates is proposed that facilitates the efficient simulation of the non-isothermal lithium-ion pseudo 2-D battery model. The transformed model is then conveniently discretized using orthogonal collocation with the collocation points in the spatial direction. The resulting system of differential algebraic equations (DAEs) is solved using efficient adaptive solvers in time. A series of mathematical operations are performed to reformulate the model to enhance computational efficiency and programming convenience while maintaining accuracy even when non-linear or temperature dependent parameters are used. The transformed coordinate allows for efficient simulation and extension from cell sandwich to stack models. Furthermore, the transformation and reformulation techniques are used to simulate operation of an 8-cell battery stack subject to varying heat transfer coefficients as well as specified temperature boundary conditions.
 [DOI: 10.1149/2.058112jes] 

Manuscript submitted March 21, 2011; revised manuscript received August 11, 2011. Published November 14, 2011; publisher error corrected November 29, 2011.

Mathematical modeling and simulation of the operation of lithium-ion batteries is not trivial, as concentration and potential fields must be evaluated simultaneously in both solid and liquid phases. This is complicated by the fact that the transport and kinetic parameters which determine battery behavior are highly nonlinear, leading to very complex governing equations. Doyle et al.[1] developed a general model based on concentrated solution theory to describe the internal behavior of a lithium-ion sandwich consisting of positive and negative porous electrodes, a separator, and current collectors.[2] This model proved generic enough to incorporate further advancements in battery systems understanding, leading to the development of a number of similar models.[3–13] Reviews of models for lithium-ion batteries can be found elsewhere in the literature.[10–12] Table I depicts a pseudo-two-dimensional isothermal model for a lithium-ion battery.[14–16] Table II presents the various expressions used in the model, while Table III shows the physical parameters used in this paper. For analysis and control of lithium-ion batteries in hybrid environments (e.g. with a fuel cell, capacitor, or other electrical components), there is a need to simulate state of charge, state of health, and other parameters of lithium-ion batteries in milliseconds. Full-order physics-based models may simulate discharge curves in several seconds to minutes, depending on the solvers, routines, computers, etc. In contrast, empirical models (based on correlations of past data) can simulate specific operating scenarios in milliseconds. However, use of these models under a different operating condition than for which they were developed may cause abuse or underutilization of electrochemical power sources. This paper presents a coordinate transformation and mathematical analysis for reformulation of physics-based models to solve them quickly, conveniently, and accurately in a way that is valid for a wide range of operating conditions and parameters.

The porous electrode model as given in Table I is a physics-based first principles model that describes the behavior of a 1-D battery subject to isothermal conditions. This is a system of ten partial differential equations (PDEs) in one linear coordinate, $x$, the radial coordinate, $r$, and the temporal coordinate, $t$, which must be solved simultaneously. The first equation is derived from concentrated solution theory and material balances. The second equation is the charge balance in the liquid phase while the third equation is the charge balance in the solid phase. The fourth equation is Fick's law of diffusion inside the solid particles (solid phase). These equations must be applied to each region individually, while noting that there is no active solid phase in the separator region.

In order to simplify the model, the radial dependence of the solid phase concentration can be eliminated by using a polynomial profile approximation.[14] Rather than representing the solid phase concentration as a continuous function of $x$, $r$ and $t$, the solid phase is represented by the particle surface concentration and the particle average concentration, both of which are functions of the linear spatial coordinate and time only. This type of volume-averaging[17,18] combined with the polynomial approximation[19,20] has been shown to be accurate for low to medium rates of discharge.[21–25] This step eliminates equations 1.4 and 1.10 from Table I and results in the following equations for the average and surface solid phase concentration:

$$\frac{\partial}{\partial t} c_i^{s,avg} = -3\frac{j_i}{R_i} \qquad [1]$$

$$\frac{D_{s,i}}{R_i}(c_i^{s,surf} - c_i^{s,avg}) = -\frac{j_i}{5} \quad i = p, n \qquad [2]$$

where the subscript $i$ refers to either the positive or negative electrode. This step results in a total of 12 equations that must be solved across the three regions: the positive and negative electrodes, and the separator. Although this reformulation results in a net gain of two additional equations that must be solved, it is computationally advantageous because there are now only two independent variables ($x$ and $t$) that must be accounted for rather than three ($x$, $r$, and $t$). Note that the polynomial profile approximation is not valid at high rates or short times; it is efficient at long times and for low to moderate rates of charging/discharging, and hence is used in this paper for demonstration purposes. For higher rates of discharge, a different approximation for the solid phase concentration must be used in order to maintain accuracy. Several such approaches can be found in the literature.[15,21–25] This paper uses the mixed finite difference approach developed by Ramadesigan, et al.[25] for simulation of discharge rates greater than 1C. The mixed finite difference approach uses 6 optimally spaced node points (with 6 corresponding governing equations) to describe the behavior of the lithium ion concentration in the radial direction within the solid phase particles. This is in contrast to the polynomial profile approximation, which relies on 2 governing equations to describe the solid phase concentration. This allows the mixed finite difference approach to better capture the dynamics within the electrode at high rates, though at the cost of additional computation time.

Typically, numerical approaches are used to solve these equations. The first of these solution approaches have included discretization

* Electrochemical Society Student Member.
** Electrochemical Society Active Member.
z E-mail: vsubramanian@seas.wustl.edu

**Table I. Governing Equations for Li-ion batteries.**

| Governing Equations | Boundary Conditions | |
|---|---|---|
| **Positive Electrode** | | |
| $\varepsilon_p \frac{\partial c}{\partial t} = \frac{\partial}{\partial x}\left[D_{\text{eff,p}} \frac{\partial c}{\partial x}\right] + a_p (1 - t_+) j_p$ | $\left.\frac{\partial c}{\partial x}\right\|_{x=0} = 0$ | (1.1) |
| | $-D_{\text{eff,p}} \frac{\partial c}{\partial x}\Big\|_{x=l_p^-} = -D_{\text{eff,s}} \frac{\partial c}{\partial x}\Big\|_{x=l_p^+}$ | |
| $-\sigma_{eff,p} \frac{\partial \Phi_1}{\partial x} - \kappa_{\text{eff,p}} \frac{\partial \Phi_2}{\partial x} + \frac{2\kappa_{\text{eff,p}} RT}{F} (1 - t_+) \frac{\partial \ln c}{\partial x} = I$ | $\left.\frac{\partial \Phi_2}{\partial x}\right\|_{x=0} = 0$ | (1.2) |
| | $-\kappa_{\text{eff,p}} \frac{\partial \Phi_2}{\partial x}\Big\|_{x=l_p^-} = -\kappa_{\text{eff,s}} \frac{\partial \Phi_2}{\partial x}\Big\|_{x=l_p^+}$ | |
| $\frac{\partial}{\partial x}\left[\sigma_{\text{eff,p}} \frac{\partial \Phi_1}{\partial x}\right] = a_p F j_p$ | $\left.\frac{\partial \Phi_1}{\partial x}\right\|_{x=0} = -\frac{I}{\sigma_{eff,p}}$ | (1.3) |
| | $\left.\frac{\partial \Phi_1}{\partial x}\right\|_{x=l_p^-} = 0$ | |
| $\frac{\partial c_p^s}{\partial t} = \frac{1}{r^2} \frac{\partial}{\partial r}\left[r^2 D_p^s \frac{\partial c_p^s}{\partial r}\right]$ | $\left.\frac{\partial c_p^s}{\partial r}\right\|_{r=0} = 0$ | (1.4) |
| | $\left.\frac{\partial c_p^s}{\partial r}\right\|_{r=R_p} = -j_p D_p^s$ | |
| **Separator** | | |
| $\varepsilon_s \frac{\partial c}{\partial t} = \frac{\partial}{\partial x}\left[D_{\text{eff,s}} \frac{\partial c}{\partial x}\right]$ | $c\|_{x=l_p^-} = c\|_{x=l_p^+}$ | (1.5) |
| | $c\|_{x=l_p+l_s^-} = c\|_{x=l_p+l_s^+}$ | |
| $-\kappa_{\text{eff,s}} \frac{\partial \Phi_2}{\partial x} + \frac{2\kappa_{\text{eff,s}} RT}{F} (1 - t_+) \frac{\partial \ln c}{\partial x} = I$ | $\Phi_2\|_{x=l_p^-} = \Phi_2\|_{x=l_p^+}$ | (1.6) |
| | $\Phi_2\|_{x=l_p+l_s^-} = \Phi_2\|_{x=l_p+l_s^-}$ | |
| **Negative Electrode** | | |
| $\varepsilon_n \frac{\partial c}{\partial t} = \frac{\partial}{\partial x}\left[D_{\text{eff,n}} \frac{\partial c}{\partial x}\right] + a_n (1 - t_+) j_n$ | $\left.\frac{\partial c}{\partial x}\right\|_{x=l_p+l_s+l_n} = 0$ | (1.7) |
| | $-D_{\text{eff,s}} \frac{\partial c}{\partial x}\Big\|_{x=l_p+l_s^-} = -D_{\text{eff,n}} \frac{\partial c}{\partial x}\Big\|_{x=l_p+l_s^+}$ | |
| $-\sigma_{\text{eff,n}} \frac{\partial \Phi_1}{\partial x} - \kappa_{\text{eff,n}} \frac{\partial \Phi_2}{\partial x} + \frac{2\kappa_{\text{eff,n}} RT}{F} (1 - t_+) \frac{\partial \ln c}{\partial x} = I$ | $\Phi_2\|_{x=l_p+l_s+l_n} = 0$ | (1.8) |
| | $-\kappa_{\text{eff,s}} \frac{\partial \Phi_2}{\partial x}\Big\|_{x=l_p+l_s^-} = -\kappa_{\text{eff,p}} \frac{\partial \Phi_2}{\partial x}\Big\|_{x=l_p+l_s^+}$ | |
| $\frac{\partial}{\partial x}\left[\sigma_{\text{eff,n}} \frac{\partial \Phi_1}{\partial x}\right] = a_n F j_n$ | $\left.\frac{\partial \Phi_1}{\partial x}\right\|_{x=l_p+l_s^-} = 0$ | (1.9) |
| | $\left.\frac{\partial \Phi_1}{\partial x}\right\|_{x=l_p+l_s+l_n} = -\frac{I}{\sigma_{eff,n}}$ | |
| $\frac{\partial c_n^s}{\partial t} = \frac{1}{r^2} \frac{\partial}{\partial r}\left[r^2 D_n^s \frac{\partial c_n^s}{\partial r}\right]$ | | (1.10) |

in both space and time.[1–5] Recently, discretization in space alone has been used by few researchers in order to take advantage of the speed gained by time-adaptive solvers such as DASSL[26] for the time coordinate.[27,28] This reduces the system of PDEs to a system of differential algebraic equations (DAEs) of index 1 with time as the only independent variable. However, this results in a very large number of nonlinear DAEs to be solved when a finite difference scheme is used. Assume that 50 equally spaced node points in the linear length scale (i.e. in $x$) are used to discretize each of the cathode, separator, and anode. The cathode now has 50 ordinary differential equations for both the electrolyte concentration and solid-phase average concentration, and 50 algebraic equations for the potential in both the electrolyte and solid phase as well as for the solid-phase surface concentration. This results in a system of 250 DAEs for the cathode. The anode is discretized in the same manner resulting in 250 additional DAEs. Since there is no active solid phase in the separator, using 50 node points will result in 50 differential equations for the electrolyte concentration and 50 algebraic equations for the electrolyte potential, for a total of 100 DAEs to describe this region. Thus, the total number of DAEs to be solved for the full-order model across the entire cell is $250 + 250 + 100 = 600$ DAEs.

Given the large number of DAEs that must be solved, the full order spatial discretization is slow and computationally inefficient. These inefficiencies are compounded when used for control or optimization,

**Table II. Additional Expressions for Li-ion batteries.**

$$j_p = 2k_p c^{0.5} c^s \Big|_{r=R_p}^{0.5} \left(c^s_{\max,p} - c^s|_{r=R_p}\right)^{0.5} \sinh\left[\frac{0.5F}{RT}\left(\Phi_1 - \Phi_2 - U_p\right)\right] \quad (2.1)$$

$$j_n = 2k_n c^{0.5} c^s|_{r=R_n}^{0.5} \left(c^s_{\max,n} - c^s|_{r=R_n}\right)^{0.5} \sinh\left[\frac{0.5F}{RT}\left(\Phi_1 - \Phi_2 - U_n\right)\right] \quad (2.2)$$

$$\kappa_{eff,i} = \varepsilon_i^{brugg_i}\left(\begin{array}{l}4.1253 \times 10^{-2} + 5.007 \times 10^{-4} c - 4.7212 \times 10^{-7} c^2 \\ +1.5094 \times 10^{-10} c^3 - 1.6018 \times 10^{-14} c^4\end{array}\right), i = p, s, n \quad (2.3)$$

$$\sigma_{eff,i} = \sigma_i(1 - \varepsilon_i - \varepsilon_{f,i}), i = p, s, n \quad (2.4)$$

$$D_{eff,i} = D\varepsilon_i^{brugg_i}, i = p, s, n \quad (2.5)$$

$$a_i = \frac{3}{R_i}\left(1 - \varepsilon_i - \varepsilon_{f,i}\right), i = p, s, n \quad (2.6)$$

$$U_p = \frac{-4.656 + 88.669\theta_p^2 - 401.119\theta_p^4 + 342.909\theta_p^6 - 462.471\theta_p^8 + 433.434\theta_p^{10}}{-1.0 + 18.933\theta_p^2 - 79.532\theta_p^4 + 37.311\theta_p^6 - 73.083\theta_p^8 + 95.96\theta_p^{10}} \quad (2.7)$$

$$\theta_p = \frac{c^s|_{r=R_p}}{c^s_{\max,p}}$$

$$U_n = 0.7222 + 0.1387\theta_n + 0.029\theta_n^{0.5} - \frac{0.0172}{\theta_n} + \frac{0.0019}{\theta_n^{1.5}} + \quad (2.8)$$

$$0.2808\exp(0.90 - 15\theta_n) - 0.7984\exp(0.4465\theta_n - 0.4108)$$

$$\theta_n = \frac{c^s|_{r=R_n}}{c^s_{\max,n}}$$

which require fast simulation to be used effectively. Therefore it is not ideal to use a direct full order finite difference approach for these purposes. There have been many approaches to simplify the battery model for efficient evaluation while attempting to maintain a high degree of accuracy. Proper orthogonal decomposition (POD) uses the full numerical solution to fit a reduced set of eigenvalues and nodes to get a meaningful solution with a reduced number of equations.[27] However, this method requires rigorous numerical solutions to build the POD reduced-order models. Also, once the operating condition is changed, the boundary conditions are modified, or if the parameter values are adjusted significantly, the POD model needs to be reconstructed.

Another method put forth by Cai et al.[29] uses orthogonal collocation on finite elements (OCFE). By doing this, they were able to obtain similar accuracy as a conventional finite volume method while

**Table III. Parameters.**

| Symbol | Parameter | Aluminum Current Collector | Positive Electrode[a] | Separator[a] | Negative Electrode[a] | Copper Current Collector | Units |
|---|---|---|---|---|---|---|---|
| $a_i$ | Particle Surface Area to Volume | | 885000 | | 723600 | | $m^2/m^3$ |
| Brugg | Bruggeman Coefficient | | 4 | 4 | 4 | | |
| $c^s_{i,\max}$ | Maximum solid phase concentration | | 51554 | | 30555 | | $mol/m^3$ |
| $c^s_{i,0}$ | Initial solid phase concentration | | 25751 | | 26128 | | $mol/m^3$ |
| $c_0$ | Initial electrolyte concentration | | 1000 | 1000 | 1000 | | $mol/m^3$ |
| $C_p$ | Specific Heat | 897 | 700[b] | 700[b] | 700[b] | 385 | J/(kg K) |
| $D$ | Electrolyte diffusivity | | $7.5 \times 10^{-10}$ | $7.5 \times 10^{-10}$ | $7.5 \times 10^{-10}$ | | $m^2/s$ |
| $D^s_i$ | Solid Phase Diffusivity | | $1.0 \times 10^{-14}$ | | $3.9 \times 10^{-14}$ | | $m^2/s$ |
| $E_a^{D^s_i}$ | Activation Energy for Temperature Dependent Solid Phase Diffusion | | 5000[b] | | 5000[b] | | J/mol |
| $E_a^{k_i}$ | Activation Energy for Temperature Dependent Reaction Constant | | 5000[b] | | 5000[b] | | J/mol |
| $F$ | Faraday's Constant | | | 96487 | | | C/mol |
| $k_i$ | Reaction Rate constant | | $2.334 \times 10^{-11}$ | | $5.031 \times 10^{-11}$ | | $m^{2.5}/(mol^{0.5}\ s)$ |
| $l_i$ | Region thickness | $10\times10^{-6}$ [b] | $80\times10^{-6}$ | $25\times10^{-6}$ | $88\times10^{-6}$ | $10\times10^{-6}$ [b] | m |
| $R_{p,i}$ | Particle Radius | | $2.0\times10^{-6}$ | | $2.0\times10^{-6}$ | | m |
| $R$ | Gas Constant | | | 8.314 | | | J/(mol K) |
| $T_{ref}$ | Temperature | | | 298.15 | | | K |
| $t_+$ | Transference number | | | 0.364 | | | |
| $\varepsilon_{f,i}$ | Filler fraction | | 0.025 | | 0.0326 | | |
| $\varepsilon_i$ | Porosity | | 0.385 | 0.724 | 0.485 | | |
| $\lambda$ | Thermal Conductivity | 237 | 2.1[c] | 0.16[c] | 1.7[c] | 401 | J/(m K) |
| $\rho_i$ | Density | 2700 | 2500[b] | 1100[b] | 2500[b] | 8940 | $kg/m^3$ |
| $\sigma_i$ | Solid phase conductivity | $3.55\times10^7$ | 100 | | 100 | $5.96\times10^7$ | S/m |

[a] Unless otherwise noted, all parameters used for the electrodes and separator are from Ref. 28.
[b] Assumed value
[c] Ref. 39

using fewer node points. Cai et al. also suggests that application of the POD reduced order model to OCFE would further enhance the computing speed. Additionally, Lee et al.,[30] used the orthogonal collocation method to numerically evaluate the electrode performance and compare with experimental results. However, that paper focused on the experimental aspects, and only on a single carbon electrode without detailed explanations for the derivation of constants to handle non-homogeneous boundary conditions. Forman et al.[31] used a quasi-linearization approximation to reduce the complexity of the porous electrode pseudo-two dimensional model. They combined this with a Padé approximation for the solid phase concentration to develop an efficient and accurate method of solving battery models.[31]

Previously, Subramanian et al.[28] reformulated the pseudo 2-D porous electrode model for galvanostatic boundary conditions. That model provided an efficient method to solve battery models in milliseconds without using a reduced order model that potentially sacrifices accuracy. This approach has proven to be useful for isothermal models, but has difficulties when non-linear properties and thermal effects are considered. The integral calculation required for Galerkin collocation becomes particularly complicated when the diffusion coefficient of the electrolyte phase is nonlinear. The approach presented in this paper addresses these issues by using orthogonal collocation and eliminating the need to perform numerical integration.

In our opinion, researchers have not used orthogonal collocation directly because (1) it is not trivial to choose trial functions for composite domains (i.e. cathode/separator/anode) and (2) the trial function should satisfy all boundary conditions, including those of flux continuity at the cathode/separator and separator/anode interfaces. This paper addresses these issues by presenting a coordinate transformation combined with an orthogonal collocation reformulation for the simulation of lithium ion battery operation. This reformulation is designed to be computationally easier to implement and efficient while maintaining the fidelity of the physics based model on which it is based.

This reformulation will achieve the goal of being computationally efficient by substantially reducing the number of DAEs that must be solved. Also, the coordinates will be transformed so that each region (cathode, anode, and separator) is a function of a dummy variable $X$ in the domain [0, 1]. Following this, the remaining equations are discretized in $X$ by using orthogonal collocation. This approach converges much faster than finite difference, thereby requiring fewer terms to obtain a meaningful result.[32] Once this is done, the system of equations will be examined to eliminate any variable that can be solved for in terms of the other variables. The physics of the system are maintained by limiting the assumptions made during the reformulation.

The coordinate transformation used in this reformulation enables the extension of the model for a single cell sandwich to a multi-cell stack. The robustness of the proposed reformulation is shown by simulating an electrochemical thermal coupled multi-cell stack model. The inclusion of temperature increases the computational load by adding an additional dependent variable and including non-constant and non-linear parameters in the model. This thermal simulation is performed in context of a multi-cell battery stack to show the effects that an applied temperature gradient has on individual cells in a stack. This can be useful for examining the behavior of the cells within the battery under various charging and discharging scenarios.

## Coordinate Transformation

It should be noted that the original formulation of the problem has the three regions defined sequentially. In other words, the equations for the positive electrode are defined on the region $[0, l_p]$, the equations for the separator are defined on the region $[l_p, l_p+l_s]$, and the negative electrode equations are defined on the region $[l_p+l_s, l_p+l_s+l_n]$. In order to decrease the required computation, each region is rescaled to a domain of [0, 1]. This effectively reduces the problem from three regions to a single region. This is shown graphically in Figure 1.

As an example, this transformation is shown in detail for the electrolyte concentration in the cathode, separator, and anode. From Equations (1.1), (1.5), and (1.7) from Table I, the governing equations for the electrolyte concentration are:

$$\varepsilon_p \frac{\partial c}{\partial t} = \frac{\partial}{\partial x}\left[D_{\text{eff,p}} \frac{\partial c}{\partial x}\right] + a_p (1 - t_+)\, j_p \quad 0 < x < l_p \qquad [3.a]$$

$$\varepsilon_s \frac{\partial c}{\partial t} = \frac{\partial}{\partial x}\left[D_{\text{eff,s}} \frac{\partial c}{\partial x}\right] \quad l_p < x < l_p + l_s \qquad [3.b]$$

$$\varepsilon_n \frac{\partial c}{\partial t} = \frac{\partial}{\partial x}\left[D_{\text{eff,n}} \frac{\partial c}{\partial x}\right] + a_n (1 - t_+)\, j_n \quad l_p + l_s < x < l_p + l_s + l_n \qquad [3.c]$$

with the boundary conditions given as

$$\left.\frac{\partial c}{\partial x}\right|_{x=0} = 0 \qquad [4.a]$$

$$-D_{\text{eff,p}} \left.\frac{\partial c}{\partial x}\right|_{x=l_p^-} = -D_{\text{eff,s}} \left.\frac{\partial c}{\partial x}\right|_{x=l_p^+} \qquad [4.b]$$

$$c|_{x=l_p^-} = c|_{x=l_p^+} \qquad [4.c]$$

$$c|_{x=l_p+l_s^-} = c|_{x=l_p+l_s^+} \qquad [4.d]$$

$$-D_{\text{eff,s}} \left.\frac{\partial c}{\partial x}\right|_{x=l_p+l_s^-} = -D_{\text{eff,n}} \left.\frac{\partial c}{\partial x}\right|_{x=l_p+l_s^+} \qquad [4.e]$$

$$\left.\frac{\partial c}{\partial x}\right|_{x=l_p+l_s+l_n} = 0 \qquad [4.f]$$

In order to convert the three region cell to a single region, the spatial coordinate, $x$, must first be transformed to the dimensionless coordinates $X_1$, $X_2$, and $X_3$ in the anode, separator, and cathode, respectively. These transformations are achieved using the following equations:

$$X_1 = \frac{x}{l_p} \qquad [5.a]$$

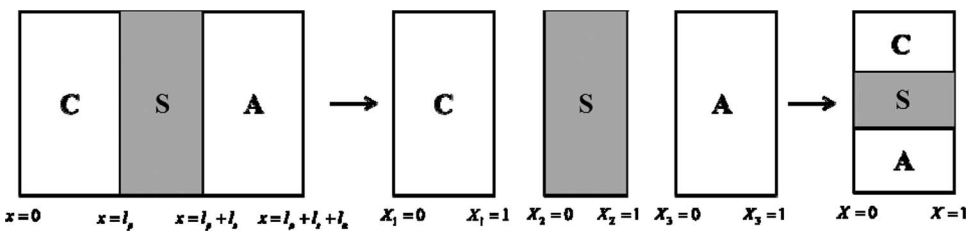


**Figure 1.** Proposed coordinate transformation for a single 1-D cell—note that the final diagram is used to show that the cathode, separator, and anode are solved in the same coordinate domain. It does not indicate that a second linear dimension is considered.

$$X_2 = \frac{x - l_p}{l_s} \quad [5.b]$$

$$X_3 = \frac{x - l_p - l_s}{l_n} \quad [5.c]$$

Equations 5.a to 5.c can be applied to Equations 3.a to 4.f to arrive at the transformed governing equations for the concentration profiles:

$$\varepsilon_p \frac{\partial c}{\partial t} = \frac{1}{l_p}\frac{\partial}{\partial X_1}\left[\frac{D_{\text{eff,p}}}{l_p}\frac{\partial c}{\partial X_1}\right] + a_p(1 - t_+)\, j_p \quad 0 < X_1 < 1 \quad [6.a]$$

$$\varepsilon_s \frac{\partial c}{\partial t} = \frac{1}{l_s}\frac{\partial}{\partial X_2}\left[\frac{D_{\text{eff,s}}}{l_s}\frac{\partial c}{\partial X_2}\right] \quad 0 < X_2 < 1 \quad [6.b]$$

$$\varepsilon_n \frac{\partial c}{\partial t} = \frac{1}{l_n}\frac{\partial}{\partial X_3}\left[\frac{D_{\text{eff,n}}}{l_n}\frac{\partial c}{\partial X_3}\right] + a_n(1 - t_+)\, j_n \quad 0 < X_3 < 1 \quad [6.c]$$

While the boundary conditions become

$$\left.\frac{\partial c}{\partial X_1}\right|_{X_1=0} = 0 \quad [7.a]$$

$$-\left.\frac{D_{\text{eff,p}}}{l_p}\frac{\partial c}{\partial X_1}\right|_{X_1=1} = -\left.\frac{D_{\text{eff,s}}}{l_s}\frac{\partial c}{\partial X_2}\right|_{X_2=0} \quad [7.b]$$

$$c|_{X_1=1} = c|_{X_2=0} \quad [7.c]$$

$$c|_{X_2=1} = c|_{X_3=0} \quad [7.d]$$

$$-\left.\frac{D_{\text{eff,s}}}{l_s}\frac{\partial c}{\partial X_2}\right|_{X_2=1} = -\left.\frac{D_{\text{eff,n}}}{l_n}\frac{\partial c}{\partial X_3}\right|_{X_3=0} \quad [7.e]$$

$$\left.\frac{\partial c}{\partial X_3}\right|_{X_3=1} = 0 \quad [7.f]$$

From Equations 6.a to 7.f, it is clear that $X_1$, $X_2$, and $X_3$ are independent variables that can be replaced by a single dummy variable $X$, though we must differentiate between variables in the different regions (i.e. $c$ is replaced by $c_p$, $c_s$or $c_n$, for concentration in the positive electrode, separator, and the negative electrode, respectively).

$$\varepsilon_p \frac{\partial c_p}{\partial t} = \frac{1}{l_p}\frac{\partial}{\partial X}\left[\frac{D_{\text{eff,p}}}{l_p}\frac{\partial c_p}{\partial X}\right] + a_p(1 - t_+)\, j_p \quad 0 < X < 1 \quad [8.a]$$

$$\varepsilon_s \frac{\partial c_s}{\partial t} = \frac{1}{l_s}\frac{\partial}{\partial X}\left[\frac{D_{\text{eff,s}}}{l_s}\frac{\partial c_s}{\partial X}\right] \quad 0 < X < 1 \quad [8.b]$$

$$\varepsilon_n \frac{\partial c_n}{\partial t} = \frac{1}{l_n}\frac{\partial}{\partial X}\left[\frac{D_{\text{eff,n}}}{l_n}\frac{\partial c_n}{\partial X}\right] + a_n(1 - t_+)\, j_n \quad 0 < X < 1 \quad [8.c]$$

With the boundary conditions

$$\left.\frac{\partial c_p}{\partial X}\right|_{X=0} = 0 \quad [9.a]$$

$$-\left.\frac{D_{\text{eff,p}}}{l_p}\frac{\partial c_p}{\partial X}\right|_{X=1} = -\left.\frac{D_{\text{eff,s}}}{l_s}\frac{\partial c_s}{\partial X}\right|_{X=0} \quad [9.b]$$

$$c_p|_{X=1} = c_s|_{X=0} \quad [9.c]$$

$$c_s|_{X=1} = c_n|_{X=0} \quad [9.d]$$

$$-\left.\frac{D_{\text{eff,s}}}{l_s}\frac{\partial c_s}{\partial X}\right|_{X=1} = -\left.\frac{D_{\text{eff,n}}}{l_n}\frac{\partial c_n}{\partial X}\right|_{X=0} \quad [9.e]$$

$$\left.\frac{\partial c_n}{\partial X}\right|_{X=1} = 0 \quad [9.f]$$

A similar process is performed on the remaining variables and the resulting equations and boundary conditions are given in Table IV.

## Orthogonal Collocation

This paper examines the orthogonal collocation approach as applied to the porous electrode model for lithium-ion batteries. The theory of orthogonal collocation is well established and stability theory has been discussed in the literature.[32,33] In order to set up a system of DAEs, the proposed reformulation discretizes the model in the $x$-direction while maintaining the time dependence to allow for the implementation of time-adaptive solvers. In the reformulation, each variable of interest is approximated by a summation of trial functions of the form:

$$u(X,t) = F(X,t) + \sum_{k=0}^{N} B_k(t) T_k(X) \quad [10]$$

Where $u(X,t)$ is the variable of interest, $T_k(X)$ are the chosen trial functions with homogenous boundary conditions, $F(X,t)$ is a function chosen to satisfy the (time-dependent) boundary conditions, and $B_k(t)$ are the coefficients of the trial functions. The only requirement of the trial functions is that they all be linearly independent. However, the choice of trial functions does affect the accuracy of the final solution, and a proper choice can improve convergence. For this model, the homogeneous trial functions are typically selected to be cosine functions while the boundary conditions are satisfied by linear and quadratic terms. Because of the coordinate transformation discussed previously, the cosine trial functions can be applied in a simple form of $\cos(k\pi X)$ for each variable.

The approximate form of each variable is given in Table V. For the variables with non-homogeneous boundary conditions, an additional linear and/or quadratic term is added to the approximate solution to satisfy the boundary conditions. This allows the boundary conditions to be applied analytically before applying the time-adaptive DAE solver. For example, the liquid phase concentration is approximated by the equations:

$$c_p(X,t) = A_{p,c}(t)X^2 + \sum_{k=0}^{N_p} B_{p,c,k}(t)\cos(k\pi X) \quad [11]$$

$$c_s(X,t) = A_{s,c,1}(t)X + A_{s,c,2}(t)X^2 + \sum_{k=0}^{N_s} B_{s,c,i}(t)\cos(k\pi X) \quad [12]$$

$$c_n(X,t) = A_{n,c}(t)(X-1)^2 + \sum_{k=0}^{N_n} B_{n,c,k}(t)\cos(k\pi X) \quad [13]$$

for the positive electrode, the separator, and the negative electrode, respectively. For the roughest approximation, let $N_p = N_s = N_n = 1$. In this case Equations 11–13 become

$$c_p(X,t) = A_{p,c}(t)X^2 + B_{p,c,0}(t) + B_{p,c,1}(t)\cos(\pi X) \quad [14]$$

$$c_s(X,t) = A_{s,c,1}(t)X + A_{s,c,2}(t)X^2 + B_{s,c,0}(t) + B_{s,c,1}(t)\cos(\pi X) \quad [15]$$

$$c_n(X,t) = A_{n,c}(t)(X-1)^2 + B_{n,c,0}(t) + B_{n,c,1}(t)\cos(\pi X) \quad [16]$$

**Table IV. Transformed Governing Equations for Li-ion batteries.**

| Governing Equation | Boundary Conditions | |
|---|---|---|
| **Positive Electrode** | | |
| $\varepsilon_p \frac{\partial c_p}{\partial t} = \frac{1}{l_p}\frac{\partial}{\partial X}\left[\frac{D_{\text{eff,p}}}{l_p}\frac{\partial c_p}{\partial X}\right] + a_p(1-t_+)j_p$ | $\left.\frac{\partial c_p}{\partial X}\right\|_{X=0} = 0$ | (4.1) |
| | $\left.\frac{-D_{\text{eff,p}}}{l_p}\frac{\partial c_p}{\partial X}\right\|_{X=1} = \left.\frac{-D_{\text{eff,s}}}{l_s}\frac{\partial c_s}{\partial X}\right\|_{X=0}$ | |
| $\frac{-\sigma_{\text{eff,p}}}{l_p}\frac{\partial \Phi_{2,p}}{\partial X} - \frac{\kappa_{\text{eff,p}}}{l_p}\frac{\partial \Phi_{2,p}}{\partial x} + \frac{2\kappa_{\text{eff,p}}RT}{F}\frac{(1-t_+)}{l_p}\frac{\partial \ln c_p}{\partial x} = I$ | $\left.\frac{\partial \Phi_{2,p}}{\partial X}\right\|_{X=0} = 0$ | (4.2) |
| | $\left.\frac{-\kappa_{\text{eff,p}}}{l_p}\frac{\partial \Phi_{2,p}}{\partial X}\right\|_{X=1} = \left.\frac{-\kappa_{\text{eff,s}}}{l_s}\frac{\partial \Phi_{2,s}}{\partial X}\right\|_{X=0}$ | |
| $\frac{1}{l_p}\frac{\partial}{\partial X}\left[\frac{\sigma_{\text{eff,p}}}{l_p}\frac{\partial}{\partial X}\Phi_{1,p}\right] = a_p F j_p$ | $\left.\frac{1}{l_p}\frac{\partial \Phi_{1,p}}{\partial X}\right\|_{X=0} = -\frac{I}{\sigma_{eff,p}}$ | (4.3) |
| | $\left.\frac{\partial \Phi_{1,p}}{\partial X}\right\|_{X=1} = 0$ | |
| $\frac{\partial}{\partial t}c_p^{s,avg} = -3\frac{j_p}{R_p}$ | | (4.4.a) |
| $\frac{D_p^s}{R_p}\left(c_p^{s,surf} - c_p^{s,avg}\right) = -\frac{j_p}{5}$ | | (4.4.b) |
| **Separator** | | |
| $\varepsilon_s \frac{\partial c_s}{\partial t} = \frac{1}{l_s}\frac{\partial}{\partial X}\left[\frac{D_{\text{eff,s}}}{l_s}\frac{\partial c_s}{\partial X}\right]$ | $c_p\|_{X=1} = c_s\|_{X=0}$ | (4.5) |
| | $c_s\|_{X=1} = c_n\|_{X=0}$ | |
| $\frac{-\kappa_{\text{eff,s}}}{l_s}\frac{\partial \Phi_{2,s}}{\partial X} + \frac{2\kappa_{\text{eff,s}}RT}{F}\frac{(1-t_+)}{l_s}\frac{\partial \ln c_s}{\partial X} = I$ | $\Phi_{2,s}\|_{X=1} = \Phi_{2,n}\|_{X=0}$ | (4.6) |
| | $\Phi_{2,p}\|_{X=1} = \Phi_{2,s}\|_{X=0}$ | |
| **Negative Electrode** | | |
| $\varepsilon_n \frac{\partial c_n}{\partial t} = \frac{1}{l_n}\frac{\partial}{\partial X}\left[\frac{D_{\text{eff,n}}}{l_n}\frac{\partial c_n}{\partial X}\right] + a_n(1-t_+)j_n$ | $\left.\frac{\partial c_n}{\partial X}\right\|_{X=1} = 0$ | (4.7) |
| | $\left.\frac{-D_{\text{eff,s}}}{l_s}\frac{\partial c_s}{\partial X}\right\|_{X=1} = \left.\frac{-D_{\text{eff,n}}}{l_n}\frac{\partial c_n}{\partial X}\right\|_{X=0}$ | |
| $\frac{-\sigma_{\text{eff,n}}}{l_n}\frac{\partial \Phi_{1,n}}{\partial X} - \frac{\kappa_{\text{eff,n}}}{l_n}\frac{\partial \Phi_{2,n}}{\partial X} + \frac{2\kappa_{\text{eff,n}}RT}{F}\frac{(1-t_+)}{l_n}\frac{\partial \ln c_n}{\partial X} = I$ | $\Phi_{2,n}\|_{X=1} = 0$ | (4.8) |
| | $\left.\frac{-\kappa_{\text{eff,s}}}{l_s}\frac{\partial \Phi_{2,s}}{\partial X}\right\|_{X=1} = \left.\frac{-\kappa_{\text{eff,p}}}{l_n}\frac{\partial \Phi_{2,n}}{\partial X}\right\|_{X=0}$ | |
| $\frac{1}{l_n}\frac{\partial}{\partial X}\left[\frac{\sigma_{\text{eff,n}}}{l_n}\frac{\partial}{\partial X}\Phi_{1,n}\right] = a_n F j_n$ | $\left.\frac{\partial \Phi_{1,n}}{\partial X}\right\|_{X=0} = 0$ | (4.9) |
| | $\left.\frac{1}{l_n}\frac{\partial \Phi_{1,n}}{\partial X}\right\|_{X=1} = -\frac{I}{\sigma_{eff,n}}$ | |
| $\frac{\partial}{\partial t}c_n^{s,avg} = -3\frac{j_n}{R_n}$ | | (4.10.a) |
| $\frac{D_n^s}{R_n}\left(c_n^{s,surf} - c_n^{s,avg}\right) = -\frac{j_n}{5}$ | | (4.10.b) |

It should be pointed out that there are no lithium ions leaving or entering the cell sandwich, so the flux at both ends of the cell is set to zero. These boundary conditions are included in the original form above by choosing the linear and quadratic terms appropriately. For example, in Equation 11 there is no linear term for the concentration of the electrolyte in the positive electrode so that the derivative, $\frac{\partial}{\partial X}c_p(X,t)$, is zero at the current collector located at $X = 0$, while holding no such restrictions at the positive electrode-separator interface. Similarly, the $(X-1)^2$ term accomplishes the same effect in Equation 13 for the negative electrode. The equations given in Table V have been developed by considering the boundary conditions for each variable in the same manner as described above. The coefficients of the linear and quadratic terms, $A_{r,v,i}(t)$ (where $r$, $v$ and $i$ denote the region, variable, and term to which the coefficient applies), are determined by requiring that each variable be continuous at both electrode-separator interfaces, while also maintaining a continuous flux.

By applying the continuity boundary conditions, it is possible to analytically solve for these coefficients simultaneously in terms of the coefficients of the trial functions. This is shown below for the positive electrode in which only a single cosine term is used, though this procedure can be applied for any number of trial functions used,

**Table V. Approximate forms of Equations.**

**Positive Electrode**

$$c_p(X,t) = A_{p,c}(t)X^2 + \sum_{k=0}^{N_p} B_{p,c,k}(t)\cos(k\pi X) \tag{5.1}$$

$$\Phi_{2,p}(X,t) = A_{p,\Phi_2}(t)X^2 + \sum_{k=0}^{N_p} B_{p,\Phi_2,k}(t)\cos(k\pi X) \tag{5.2}$$

$$\Phi_{1,p}(X,t) = \frac{i_{app}l_p}{\sigma_{eff,p}}\left[\frac{1}{2}X^2 - X\right] + \sum_{k=0}^{N_p} B_{p,\Phi_1,k}(t)\cos(k\pi X) \tag{5.3}$$

$$c_p^{s,surf}(X,t) = \sum_{k=0}^{N_p} B_{p,c^{s,surf},k}(t)\cos(k\pi X) \tag{5.4}$$

$$c_p^{s,avg}(X,t) = \sum_{k=0}^{N_p} B_{p,c^{s,avg},k}(t)\cos(k\pi X) \tag{5.5}$$

**Separator**

$$c_s(X,t) = A_{s,c,1}(t)X + A_{s,c,2}(t)X^2 + \sum_{k=0}^{N_s} B_{s,c,k}(t)\cos(k\pi X) \tag{5.6}$$

$$\Phi_{2,s}(X,t) = A_{s,\Phi_2,1}(t)X + A_{s,\Phi_2,2}(t)X^2 + \sum_{k=0}^{N_s} B_{s,\Phi_2,k}(t)\cos(k\pi X) \tag{5.7}$$

**Negative Electrode**

$$c_n(X,t) = A_{n,c}(t)(X-1)^2 + \sum_{k=0}^{N_n} B_{n,c,k}(t)\cos(k\pi X) \tag{5.8}$$

$$\Phi_{2,n}(X,t) = A_{n,\Phi_2}(t)(X-1)^2 + \sum_{k=0}^{N_n} B_{n,\Phi_2,k}(t)\cos\left[\left(k+\frac{1}{2}\right)\pi X\right] \tag{5.9}$$

$$\Phi_{1,n}(X,t) = -\frac{i_{app}l_n}{\sigma_{eff,n}}\left[\frac{1}{2}X^2\right] + \sum_{k=0}^{N_n} B_{n,\Phi_1,k}(t)\cos(k\pi X) \tag{5.10}$$

$$c_n^{s,surf}(X,t) = \sum_{k=0}^{N_n} B_{n,c^{s,surf},k}(t)\cos(k\pi X) \tag{5.11}$$

$$c_n^{s,avg}(X,t) = \sum_{k=0}^{N_p} B_{n,c^{s,avg},k}(t)\cos(k\pi X) \tag{5.12}$$

for every region, and for every variable of interest. For example, it can be shown that the coefficient of the quadratic term from Equation 14 is related to the remaining coefficients by

$$A_{p,c}(t) = -B_{p,c,0}(t) + B_{p,c,1}(t) + B_{s,c,0}(t) + B_{s,c,1}(t) \tag{17}$$

Therefore the concentration equation for the positive electrode can be written as:

$$c_p(X,t) = (-B_{p,c,0}(t) + B_{p,c,1}(t) + B_{s,c,0}(t) + B_{s,c,1}(t))X^2 + B_{p,c,0}(t) + B_{p,c,1}(t)\cos(\pi X) \tag{18}$$

This process is then repeated for each of the other unknowns ($\Phi_1$, $\Phi_2$, $c^{s,avg}$) in each electrode, and the separator, when applicable. The final form of the approximated solutions (including solving for the $A_{r,v,i}(t)$'s in terms of the $B_{r,v,i}(t)$'s) are not shown due to the large number of terms present as each $A_{r,v,i}(t)$ may be a function of up to six $B_{r,v,i}(t)$'s when using a single cosine term.

The coefficients of the trial function, $B_{r,v,i}(t)$, must be determined in order to give the best possible approximation of the solution to the twelve governing equations. The residual of a differential equation can be used to quantitatively determine the best solution. For any differential equation, or system of differential equations, of the form

$$D[y(x)] = 0 \tag{19}$$

The residual for an approximate solution is defined as

$$D[y_{approx}(x)] = R(x) \tag{20}$$

In other words, the residual is the deviation of an approximate solution from exactly satisfying a differential equation. For the porous electrode pseudo 2-D battery model examined in this paper, 12 governing equations must be satisfied, and as such there will be 12 such residuals, obtained by applying the approximate solution to the governing equations. Since these approximations are not exact, the best way to minimize the residuals while maintaining computational efficiency must be determined. This allows an adequate number of equations to be developed in order to solve for the best possible series coefficients. In order to accomplish these goals, consider the "Method of Weighted Residuals."[33] This method solves for the coefficients, $B_{r,v,i}(t)$, by setting the integral of the residual multiplied by a weight function to zero. Mathematically:

$$\int_v^R (B_{r,v,j}(t), X)W_{v,j}(X)\,dX = 0 \quad v = \Phi_1, \Phi_2, c, c^{s,surf}, c^{s,avg} \quad j = 0 \ldots N_r \quad r = p, s, n \tag{21}$$

where $R_v(B_{r,v,j}(t), X)$ is the residual for the governing equation for variable $v$, $W_{v,j}(X)$ is the $j$th weight function used for variable, $v$, and $N_r$ is the number of cosine terms used for approximation in the $r$th region. It should be noted here that there is no requirement that the variables in different regions be approximated by the same number of terms. However, all the variables in a single region must be represented by the same number of terms. For example, if the concentration profile in the positive electrode is approximated using two cosine terms, the liquid and solid phase potentials must also be approximated by two cosine terms in the positive electrode, but the concentration profile in the separator may be represented by any number of terms.

By using the method of weighted residuals, we now have a way of creating a sufficient number of differential algebraic equations to solve for all of the time dependent coefficients. However, the form of an appropriate weighting function must be determined in order achieve reasonable computing speed.[32,33] Since the integration of the weighted residuals can provide significant computational difficulties, eliminating the integral in Equation 21 would reduce the simulation time of the battery models. Therefore, the weighting functions were selected to be Dirac Delta functions:

$$W_{v,j}(X) = \delta(X_j) \quad [22]$$

The mean weighted residual becomes the residual evaluated at a point $X_j$:

$$R_v(B_{r,v,i}(t), X_j) = 0 \quad [23]$$

The governing differential equations are exactly satisfied at these collocation points. This is called the collocation method. The location of these collocation points can have a significant impact on the accuracy of the approximation, even when the same number of points is used.[32,33] The best possible approximation is found by choosing the collocation points as zeros of a specific class of orthogonal polynomials called the Jacobi polynomials, which defines the orthogonal collocation method.[32,33] The Jacobi polynomials are given by the relation:

$$P_N^{(\alpha,\beta)}(x) = \sum_{k=0}^{N} (-1)^{N-k} \gamma_k x^k \quad [24]$$

Where $\gamma_0 = 1$ and $\gamma_i$ is given by the recurrence relation:

$$\gamma_k = \frac{N-k+1}{k} \frac{N+k+\alpha+\beta}{k+\beta} \gamma_{k-1} \quad [25]$$

For a Jacobi polynomial of order $M$, there are $M$ zeros in the interval [0,1]. Since there are $N_r + 1$ coefficients for each variable in each region, a Jacobi polynomial of order $N_r + 1$ must be used to develop enough collocation equations. $\alpha$ & $\beta$ are characteristic parameters of the Jacobi polynomial. A trial and error approach found that $\alpha = \beta = 0$ minimized the error of the discharge curve relative to the finite difference approach for most simulations. However, at high rates of discharge and high node points, oscillations were observed as a result of numerical instabilities. This instability was eliminated by using $\alpha = \beta = 1$ for a 5C discharge and $\alpha = \beta = 2$ for a 10C discharge.

Once the zeros are determined for the Jacobi polynomials of interest, the residual at each collocation point can be set to 0 as in Equation 23. In development of the DAEs to be used to solve for the coefficients, each governing equation must be accounted for individually so that there are as many residual equations for each governing equation as there are coefficients to be solved in that region. For instance, if the variables in the positive electrode are represented by a single cosine term, the average solid phase concentration is approximated by

$$c_p^{s,avg}(X,t) = B_{p,c^{s,avg},0}(t) + B_{p,c^{s,avg},1}(t)\cos(\pi X) \quad [26]$$

Therefore a 2nd order Jacobi polynomial is required to find two collocation points to solve for the two unknowns, $B_{p,c^{s,avg},0}(t)$ & $B_{p,c^{s,avg},1}(t)$. Since all variables in the positive electrode ($\Phi_{1,p}$, $\Phi_{2,p}$, $c_p$, $c_p^{s,surf}$, $c_p^{s,avg}$) are approximated using the same number of terms, the same collocation points are used in each residual. The residuals are calculated using each of the five governing equations in the positive electrode. Since each residual is defined to be zero at two node points from the orthogonal collocation method, we have now developed a system of 10 DAEs to solve for the 10 unknown coefficients in the positive electrode. This must be repeated for each of the other two regions as well. In the case that each variable in all three regions are approximated by a single cosine term, there are 10 DAEs in both the positive and negative electrodes, and four DAEs in the separator for a total of 24 coupled DAEs that must be solved simultaneously.

In general terms, the dependent variables in the positive electrode, the separator, and the negative electrodes are represented by $N_p$, $N_s$, and $N_n$ cosine terms respectively. Each variable thus has $N_r + 1$ coefficients that must be determined in each region, where $r$ denotes the region, and therefore $N_r + 1$ residuals must be calculated. This results in $N_r + 1$ DAEs for each variable. Since there are 5 governing equations (and 5 variables) for the positive and negative electrodes and 2 governing equations in the separator we have a total of $5(N_p + 1) + 2(N_s + 1) + 5(N_n + 1)$ DAEs that must be solved simultaneously.

These equations are functions of time only, some of which are ordinary differential equations in time, while the remaining are algebraic equations. Solving this system is not trivial, and the algebraic variables must be initialized prior to solving to ensure that the initial conditions are consistent with the governing algebraic equations, and is a reason numerical simulations often fail for battery models. Once this is done, this system can be solved using FORTRAN with the help of time-adaptive solvers such as DASSL or DASKR.[26,28]

Once the coefficients are determined, the unknown variables are represented by continuous functions valid at any position in the cell. This is in contrast to a solution obtained using a finite difference approach in which the variable is only determined at discrete node points and would require interpolation methods to find the solution between two node points. Also, orthogonal collocation converges to a solution with an error on the order of $h^{2N}$, where $N$ is the number of collocation points and $h$ is the node spacing.[32] The finite difference solution that is typically used has an error on the order of $h^2$. Although the resulting equations are more complicated when using orthogonal collocation, fewer terms are required for a meaningful solution, resulting in fewer DAEs that must be solved and a net reduction in computation time.[32]

This proposed reformulation makes no assumptions of the form of any parameter used in any of the equations. There are no requirements that the diffusion coefficients, nor the conductivities, are constant or linear, and successful results have been obtained by using diffusion coefficients which are functions of the electrolyte concentration and temperature. This model is also versatile enough to work under galvanostatic, potentiostatic, and constant power conditions, even for continuous cell charge-discharge cycles. This model also does not assume a particular chemistry and has proven to be robust for different chemistries involving a variety of open circuit potentials and battery design parameters. Importantly, as we have chosen the polynomials in the region 0 to 1, globally convergent profiles can be obtained for any condition by increasing the number of terms in the series.

## Reformulation

Further reformulations can be done to improve computation time by eliminating the need to numerically solve for the solid phase surface concentration while using the polynomial approximation for the solid phase. Once the remaining variables have been approximated by a series solution, it is possible to analytically solve for $c_s^{surf}$ in terms of these variables. First, the pore wall flux, $j_i$, can be determined from Equation 2 above to give.

$$j_i = -5\frac{D_{solid,i}}{R_i}\left(c_i^{s,surf} - c_i^{s,avg}\right) \quad [27]$$

This form can be inserted into Equations 1.3 and 1.9 from Table I (for the positive and negative electrodes, respectively) to give the

following equation:

$$\sigma_{eff,i}\frac{\partial^2\Phi_1}{\partial x^2} = -a_i F\frac{5D_i^s}{R_i}\left(c_i^{s,surf} - c_i^{s,avg}\right) \quad [28]$$

From this the surface concentration can be solved in terms of the average solid phase concentration and the solid phase potential:

$$c_i^{s,surf} = c_i^{s,avg} - \frac{\sigma_{eff,i}R_i}{5a_i F D_i^s}\frac{\partial^2\Phi_1}{\partial x^2} \quad [29]$$

At this point, the focus will be limited to the positive electrode for demonstration purposes. The solid phase potential, $\Phi_{1,p}$, and solid phase average concentration, $c_p^{s,avg}$, each have a series solution given by

$$\Phi_{1,p} = \frac{i_{app}l_p}{\sigma_{eff,p}}\left[\frac{1}{2}X^2 - X\right] + \sum_{k=0}^{N_p} B_{p,\Phi_1,k}(t)\cos(k\pi X) \quad [30]$$

$$c_p^{s,avg} = \sum_{k=0}^{N_p} B_{p,c_p^{s,avg},k}(t)\cos(k\pi X) \quad [31]$$

By inserting Equations 30 and 31 into Equation 29, the solid phase surface concentration can be immediately written as

$$c_p^{s,surf} = -\frac{R_p i_{app}}{5a_p F D_i^s l_p} + B_{p,c^{s,avg},0}(t) + \sum_{k=1}^{N_p}\left\{B_{p,c^{s,avg},k}(t) - \frac{\sigma_{eff,p}R_p k^2\pi^2}{5a_p F D_i^s l_p^2}B_{p,\Phi_1,k}(t)\right\}\cos(k\pi X) \quad [32]$$

By solving for the surface concentration analytically in terms of the other variables, we can eliminate the need to solve for two of the twelve unknowns (one from each electrode), resulting in fewer DAEs that must be solved. However, if the solid phase conductivity, $\sigma_{eff,i}$, is a function of $x$ or is nonlinear, this reformulation cannot be performed.

## Development of a Coupled Thermal Electrochemical Multi-Cell Stack Model

In order to more accurately simulate battery operation, the model can be improved by considering thermal effects and to study multiple cells arranged in a stack configuration. This increases the complexity and fidelity of the model by including more physical phenomena. Bernardi et al.[34] used an energy balance to develop a general thermal model for battery operation by considering the various modes of heat generation within the cell. Other researchers have built upon this model by incorporating heat generation effects during battery discharge for specific systems and conditions.[35–38] Kumaresan et al.[39] used the model developed by Gu and Wang[38] to couple temperature to other variables for a single cell and validated the model with the results obtained experimentally.

Pals and Newman[40] modeled the temperature profile of a multi-cell stack by simulating the behavior of a single cell, with lithium foil as the anode, to determine the rate of heat generation and different temperatures and states of charge. They then modeled a full stack by considering the effect of heat transfer between cells in the stack by using an approximation for the heat generation in each cell. In this way, the individual cells were decoupled and the calculations for an individual cell were performed independently of the temperature calculation for the entire stack.[40] Chen and Evens[41,42] performed a thermal analysis of a lithium-ion battery stack in the context of preventing thermal runaway reactions. However, they simplified the model by incorporating empirical discharge data and constant physical parameters into the model.

The simulation presented in this paper maintains the coupling between all the cells within the stack and the full physics based model with temperature varying properties, and heat generation and discharge for each cell are calculated simultaneously. The equations used for the thermal model are identical to those given in Table I with the addition of three more governing equations to model the temperature in three regions, as well as nonlinear electrolyte diffusion and electrolyte conductivity coefficients which are functions of concentration and temperature, based on work done by Valøen et al.[43] These additional equations are shown in Tables VI and VII. This is computationally difficult and an efficient method is required for simulation, and we believe this has slowed the development of such a stack model. Further complications also arise due to the presence of current collectors located between each pair of cell sandwiches, as well as at both ends of the battery stack. These current collectors provide additional thermal mass to the system which can slow the heating of the battery and should be considered in any comprehensive thermal stack model.

The same orthogonal collocation and reformulation solution method presented above for the isothermal battery simulation was used for reformulation of the thermal model for a battery stack. The coordinate transformation described above makes it possible to add multiple cells to a stack. The inclusion of current collectors in the model increases the number of regions which are considered without a significant increase in the number of variables. A challenge in the transformation occurs because there is one more current collector than there are cells; there is not a one-to-one correspondence between the current collectors and cell sandwiches. The transformation is achieved by considering the current collectors as additional regions in which only the temperature variable is considered. The only other variable which is applicable in the current collector is the solid phase potential, which is assumed to be constant and equal to the end point potentials of the adjacent electrodes. The primary challenge arises in formulating the equations and boundary conditions in a consistent manner in the battery stack. However, once this is accomplished, there is very little numerical difficulty in solving the resulting equations.

The approximate expressions for temperature were developed in the same way as the other variables and are given in Table VIII. Both linear and quadratic terms are included in these approximate expressions in order to maintain generality so that various thermal boundary conditions can be used, such as constant temperature, constant flux, or convection, as well as continuity of temperature and of heat flux between the regions. The current collectors are approximated in a similar manner. Since the current collectors are constructed of highly conductive materials, the temperature does not vary significantly across the current collectors, and no cosine terms are needed for an accurate approximation. A single constant term is adequate and must be solved for using the governing heat equation. The inclusion of the current collectors minimally increases the computational load, as only a small number of variables are added. For example, an eight-cell stack has 298 DAEs that must be solved for if current collectors are ignored. That increases to 307 DAEs when the temperature within the current collectors is considered.

Model simulation of full battery stacks provides additional challenges which can be addressed by using this reformulation and orthogonal collocation followed by a numerical solution to solve the time dependence. It is necessary to consider a full multi-cell battery stack when thermal effects are included, as a temperature profile across the battery can affect cell performance. In the case of isothermal operation, each cell is exposed to the exact same conditions which cause each individual cell to behave identically. If this symmetry is broken, for instance by forcing a temperature gradient across the cell stack, the cells may behave differently from each other.

A schematic of an $N$-cell stack is given in Figure 2a, where each anode-separator-cathode group constitutes a single cell, with aluminum current collectors located between adjacent cathodes and copper current collectors located between adjacent anodes. Note that both electrodes at the end of the stack are anodes, and each successive cell reverses the order of the electrodes. In this configuration, the cells are connected in parallel so that the same voltage is applied at each cell. Therefore, if a constant current discharge is applied to the entire battery stack, the current provided by each individual cell may vary with time. At the boundaries between the electrodes and current col-

**Table VI. Additional governing equations for thermal battery model with applied temperature boundary conditions.**

| Governing Equation | Boundary Conditions | |
|---|---|---|
| **Positive Current Collector** | | |
| $\rho_{Al}C_{p,Al}\frac{\partial T_{Al}}{\partial t} = \frac{1}{l_{cc}}\frac{\partial}{\partial X}\left[\frac{\lambda_{Al}}{l_{cc}}\frac{\partial T_{Al}}{\partial X}\right] + \frac{i_{app}^2}{\sigma_{Al}}$ | $-\frac{\lambda_{Al}}{l_{Al}}\frac{\partial T_{Al}}{\partial X}\Big\|_{X=1} = -\frac{\lambda_p}{l_p}\frac{\partial T_p}{\partial X}\Big\|_{X=0}$<br>$-\frac{\lambda_{Al}}{l_{Al}}\frac{\partial T_{Al}}{\partial X}\Big\|_{X=0} = -\frac{\lambda_p}{l_p}\frac{\partial T_p}{\partial X}\Big\|_{X=0}$ | (6.1) |
| **Positive Electrode** | | |
| $\rho_p C_{p,p}\frac{\partial T_p}{\partial t} = \frac{1}{l_p}\frac{\partial}{\partial X}\left[\frac{\lambda_p}{l_p}\frac{\partial T_p}{\partial X}\right] + Q_{\text{rxn,p}} + Q_{\text{rev,p}} + Q_{\text{ohm,p}}$ | $T_p\big\|_{X=0} = T_{Al}\big\|_{X=1}$<br>$-\frac{\lambda_p}{l_p}\frac{\partial T_p}{\partial X}\Big\|_{X=1} = -\frac{\lambda_s}{l_s}\frac{\partial T_s}{\partial X}\Big\|_{X=0}$ | (6.2) |
| **Separator** | | |
| $\rho_s C_{p,s}\frac{\partial T_s}{\partial t} = \frac{1}{l_s}\frac{\partial}{\partial X}\left[\frac{\lambda_s}{l_s}\frac{\partial T_s}{\partial X}\right] + Q_{\text{ohm,s}}$ | $T_p\big\|_{X=1} = T_s\big\|_{X=0}$<br>$T_s\big\|_{X=0} = T_n\big\|_{X=1}$ | (6.3) |
| **Negative Electrode** | | |
| $\rho_n C_{p,n}\frac{\partial T_n}{\partial t} = \frac{1}{l_n}\frac{\partial}{\partial X}\left[\frac{\lambda_n}{l_n}\frac{\partial T_n}{\partial X}\right] + Q_{\text{rxn,n}} + Q_{\text{rev,n}} + Q_{\text{ohm,n}}$ | $-\frac{\lambda_s}{l_s}\frac{\partial T_s}{\partial X}\Big\|_{X=1} = -\frac{\lambda_n}{l_n}\frac{\partial T_n}{\partial X}\Big\|_{X=0}$<br>$T_n\big\|_{X=1} = T_{Cu}\big\|_{X=0}$ | (6.4) |
| **Negative Current Collector** | | |
| $\rho_{Cu}C_{p,Cu}\frac{\partial T_{Cu}}{\partial t} = \frac{1}{l_{Cu}}\frac{\partial}{\partial X}\left[\frac{\lambda_{Cu}}{l_{Cu}}\frac{\partial T_{Cu}}{\partial X}\right] + \frac{i_{app}^2}{\sigma_{Cu}}$ | $-\frac{\lambda_n}{l_n}\frac{\partial T_n}{\partial X}\Big\|_{X=1} = -\frac{\lambda_{Cu}}{l_{Cu}}\frac{\partial T_{Cu}}{\partial X}\Big\|_{X=0}$<br>$T_{Cu}\big\|_{X=1} = T_{app}$ | (6.5) |

lectors, the electrolyte concentration is considered to have zero flux, whereas the temperature and heat flux are continuous. Additionally, the solid phase potential drop between the anode/current collector interface and the cathode/current collector interface is the same across all cells. This couples the behavior of each cell, so that all cells in the stack must be solved simultaneously. Because of the large number of equations that arise from the coupled thermal electrochemical multi-cell stack model, reformulation was performed to reduce the number of DAEs for efficient simulation.

In order to perform the stated transformation on an $N$-cell stack with current collectors, it was necessary to mathematically treat alternating cell sandwiches differently. For the odd numbered cells, the entire sandwich consisted of a total of five regions: a copper current collector, the anode, the separator, the cathode, and an aluminum current collector. The even numbered cells only consisted of the cathode, the separator, and the anode. Additionally, the odd numbered cells were flipped so that they were orientated in a cathode-separator-anode configuration so that all cells are consistent. A final copper current collector (which is present regardless of the size of the stack) was considered independently of the individual cells. This results in a system as shown in Figure 2b for a 4-cell stack, in which the positive electrode for each cell is defined on the region $[0, l_p]$, the separator on the region $[l_p, l_p+l_s]$, and the negative electrode on the region $[l_p+l_s, l_p+l_s+l_n]$ (the current collectors, where applicable, are considered outside of this range). This simplifies the problem by eliminating the need to keep track of the location and orientation of each cell in the entire stack during simulation. For the interior cells, the boundary conditions at each end of each cell are determined by continuity. It must be noted that the application of the continuity of flux requires the direction of the flux to be reversed in adjacent cells to account for flipping every other cell to achieve a consistent orientation. Once this is done, each cell is transformed to a single region, as shown in Figure 2b. This reduces the entire stack to a single region defined from [0, 1], and the stack can be solved in the same way as described previously.

## Results and Discussion

The model prediction obtained using a collocation reformulation using a varying number of terms is compared to a full-order finite difference solution based on 50 node points in $x$ for the electrodes and 35 node points for the separator in Figures 3, 4, and 8. The primary curve of interest is the discharge graph in Figure 3a, which shows the full-order finite difference solution, as well as three solutions obtained using the orthogonal collocation approach for a 1C rate of discharge. Figure 3b shows the residuals of the orthogonal collocation solutions relative to the finite difference solution, while Table IX shows a comparison of the root mean squared error as well as computation time. The least accurate collocation solution is obtained by using only one cosine term for each region, as shown by the dashed line in Figure 3. Progressively more accurate solutions can be obtained by using orthogonal collocation with a greater number of terms. Figure 3 also shows collocation solutions obtained using (3, 2, 3) terms (dotted line), (5, 3, 5) terms (dash-dot line), and (7, 3, 7) terms (solid line). Note that the nomenclature, $(N_p, N_s, N_n)$, is used to represent the number of cosine terms used in the positive electrode, the separator, and the negative electrode, respectively. Experimental validation of the porous electrode pseudo-2D model can be found elsewhere in the literature.[3–13] Therefore an established solution method using finite difference was used to validate the reformulated model presented in this paper.

The remaining internal variables which are solved for in this reformulation cannot be experimentally determined in general. However, even without experimental validation, the ability to predict the behavior of these internal variables is critical for complete understanding of the lithium ion battery. Factors such as state of charge and state of health can be determined from this model to give a prediction of the future behavior and future life of a battery. Figure 4 shows how these internal variables change with time at the region interfaces. These figures show the convergence of the orthogonal collocation method as more terms are used. Additionally, Figure 5a shows the

**Table VII. Additional Equations for Thermal Model.**

$$Q_{\text{rxn},i} = Fa_i j_i \left(\Phi_{1,i} - \Phi_{2,i} - U_i\right),\ i = p, n \tag{7.1}^{a}$$

$$Q_{\text{rev},i} = Fa_i j_i T_i \frac{\partial U_i}{\partial T},\ i = p, n \tag{7.2}^{a}$$

$$Q_{\text{ohm},i} = \sigma_{\text{eff},i}\left(\frac{1}{l_i}\frac{\partial \Phi_{1,i}}{\partial X}\right)^2 + \kappa_{\text{eff},i}\left(\frac{1}{l_i}\frac{\partial \Phi_{2,i}}{\partial X}\right)^2 + \frac{2\kappa_{\text{eff},i}RT_i}{F}(1-t_+^0)\frac{1}{l_i^2}\frac{1}{c_i}\frac{\partial c_i}{\partial X}\frac{\partial \Phi_{2,i}}{\partial X},\ i = p, n \tag{7.3}^{a}$$

$$Q_{\text{ohm,s}} = \kappa_{\text{eff},s}\left(\frac{1}{l_s}\frac{\partial \Phi_{2,s}}{\partial x}\right)^2 + \frac{2\kappa_{\text{eff},s}RT_s}{F}(1-t_+^0)\frac{1}{c_s}\frac{1}{l_s^2}\frac{\partial c_s}{\partial X}\frac{\partial \Phi_{2,i}}{\partial X} \tag{7.4}^{a}$$

$$D_{eff,i} = \varepsilon_i^{brugg_i} 1\times 10^{-4}\times 10^{-4.43-\frac{54}{T_i-229-5.0\times 10^{-3}c_i}-0.22\times 10^{-3}c_i},\ i = p, s, n \tag{7.5}^{b}$$

$$\kappa_i = \varepsilon_i^{brugg_i} 1.0\times 10^{-4}\times c_{e,i}\left(\begin{array}{l}-10.5+0.668\times 10^{-3}c_i+0.494\times 10^{-6}c_i^2+0.074T_i-\\ 1.78\times 10^{-5}c_iT_i-8.86\times 10^{-10}c_i^2T_i-6.96\times 10^{-5}T_i^2+2.80\times 10^{-8}c_iT_i^2\end{array}\right)^2 \tag{7.6}^{b}$$

$$U_i\left(T_i, \theta_i\right) = U_{\text{i,ref}}\left(T_{\text{ref}}, \theta_i\right) + \left(T_i - T_{\text{ref}}\right)\left[\frac{dU_i}{dT}\right]\Bigg|_{T_{\text{ref}}},\ i = p, n \tag{7.7}^{c}$$

$$\frac{dU_p}{dT} = -0.001\frac{\left[\begin{array}{l}0.199521039-0.928373822\theta_p+\\ 1.3645506890000003\theta_p^2-0.61154489399999998\theta_p^3\end{array}\right]}{\left[\begin{array}{l}(1-5.6614798869999997\theta_p+11.476361910\theta_p^2-\\ 9.824312135999998\theta_p^3+3.048755063\theta_p^4)\end{array}\right]} \tag{7.8}^{c}$$

$$\frac{dU_n}{dT} = \frac{0.001\left[\begin{array}{l}0.005269056+3.299265709\theta_n-91.79325798\theta_n^2+1004.911008\theta_n^3-5812.278127\theta_n^4+\\ 19329.7549\theta_n^5-37147.8947\theta_n^6-38379.18127\theta_n^7-16515.053088\theta_n^8\end{array}\right]}{\left[\begin{array}{l}1-48.092872270\theta_n+1017.234804\theta_n^2-10481.804190\theta_n^3+59431.30\theta_n^4-\\ 195881.6488\theta_n^5+374577.3152\theta_n^6-385821.1607\theta_n^7+165705.8597\theta_n^8\end{array}\right]} \tag{7.9}^{c}$$

$$D_{i,eff}^s = D_i^s \exp\left(-\frac{E_a^{D_i^s}}{R}\left[\frac{1}{T}-\frac{1}{T_{ref}}\right]\right), i = p, n \tag{7.10}^{a}$$

$$k_{i,eff} = k_i \exp\left(-\frac{E_a^{k_i}}{R}\left[\frac{1}{T}-\frac{1}{T_{ref}}\right]\right), i = p, n \tag{7.11}^{a}$$

[a] Ref. 39.
[b] Ref. 43
[c] Ref. 44

concentration profile across the transformed domain (i.e. the cell is solved as a single region from 0 to 1) at the end of discharge. Once this is transformed back to the original domain, the concentration profile across the entire sandwich can be determined and is shown in Figure 5b. It is important to note that the average concentration of the lithium ions in the electrolyte solution must be conserved throughout the entire simulation. Importantly, when the original equations are taken and averaged with the use of the boundary conditions (BCs), the

**Table VIII. Approximate forms of Temperature Equations.**

**Positive Current Collector**

$$T_{Al}(X,t) = A_{Al,T,1}(t)X + A_{Al,T,2}(t)X^2 + B_{Al,T}(t) \tag{8.4}$$

**Positive Electrode**

$$T_p(X,t) = A_{p,T,1}(t)X + A_{p,T,2}(t)X^2 + \sum_{k=0}^{N_p} B_{p,T,k}(t)\cos(k\pi X) \tag{8.1}$$

**Separator**

$$T_s(X,t) = A_{s,T,1}(t)X + A_{s,T,2}(t)X^2 + \sum_{k=0}^{N_s} B_{s,T,k}(t)\cos(k\pi X) \tag{8.2}$$

**Negative Electrode**

$$T_n(X,t) = A_{n,T,1}(t)X + A_{n,T,2}(t)X^2 + \sum_{k=0}^{N_n} B_{n,T,k}(t)\cos(k\pi X) \tag{8.3}$$

**Negative Current Collector**

$$T_{Cu}(X,t) = A_{Cu,T,1}(t)X + A_{Cu,T,2}(t)X^2 + B_{Cu,T}(t) \tag{8.4}$$

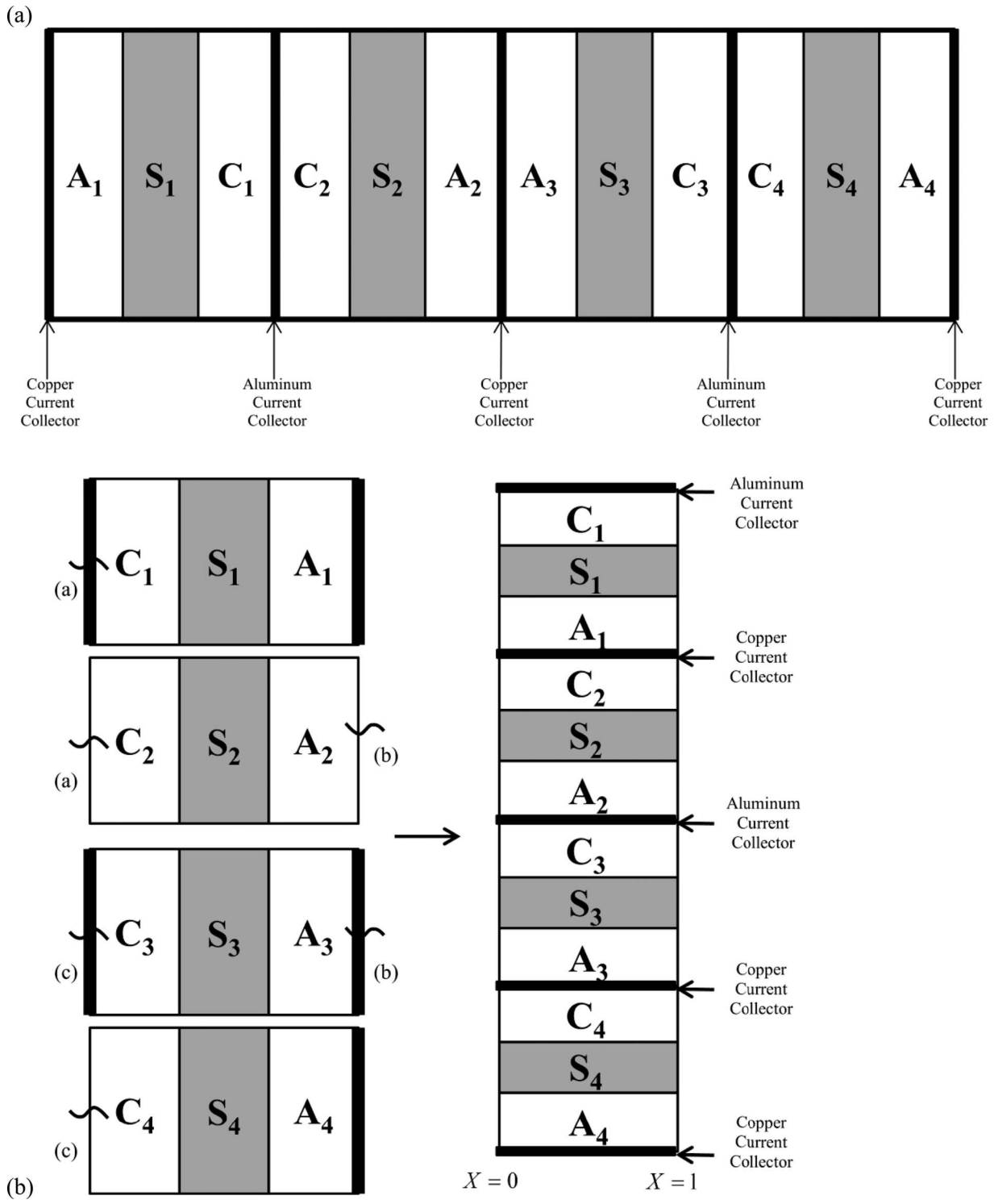


**Figure 2.** (a) Schematic for a multi-cell battery stack (b) Transformation of a 4-cell battery stack to a single cell. The letters denote connection points between adjacent cells where continuity is maintained, and the bold lines represent the current collectors. All coupled thermal electrochemical multi-cell stack simulations presented in this paper consider the effect of the current collectors when performing calculations.

mass is conserved. The collocation method presented here maintains this conservation, and there is no appreciable variation of average concentration with time.

Figures 4a and 5 show that the electrolyte concentration at the end of discharge increases across the battery from the positive electrode to the negative electrode. These figures also show that the concentration in the positive electrode decreases during discharge, while it increases in the negative electrode, as lithium metal stored in the anode comes out of the active solid particle and reacts at the surface to produce lithium-ions causing an increase in local lithium salt concentration in the electrolyte. At higher rates of discharge, more lithium ions are released at the anode and absorbed in the cathode, increasing the concentration gradient that must be overcome and limiting the capacity at high rates of discharge.

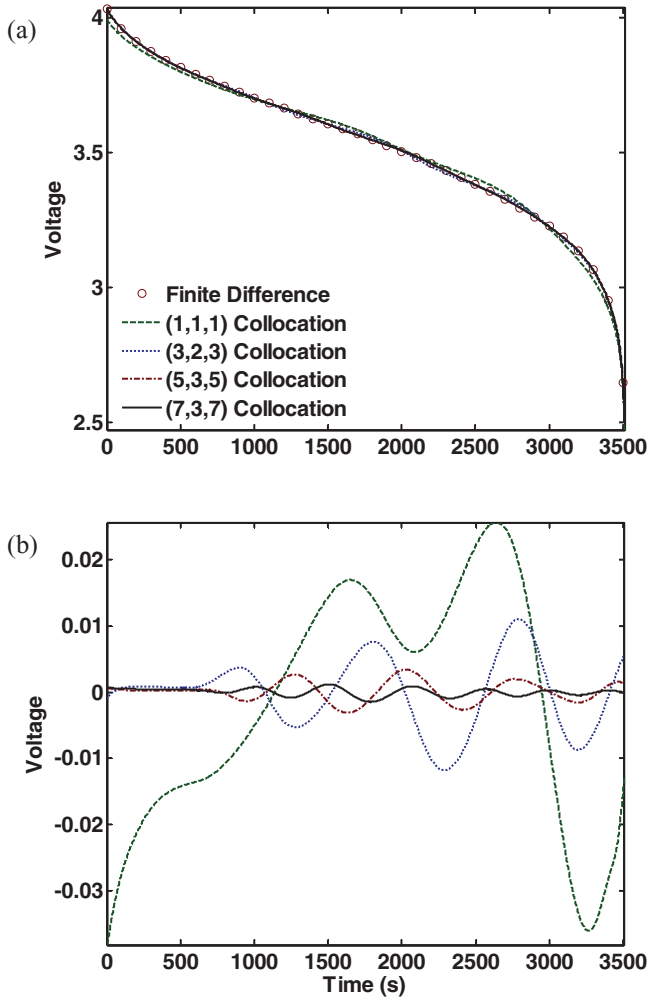


**Figure 3.** (a) Voltage-Time Curve for constant current discharge (1C) (b) Residual plot of collocation solutions vs. finite difference.

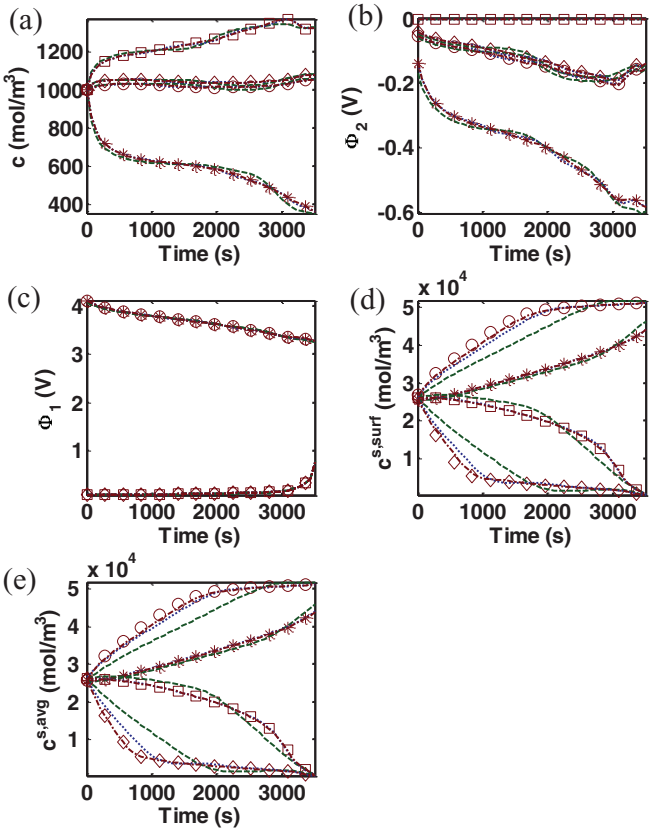


**Figure 4.** Variable values at the current collector/cathode interface (*), the cathode/separator interface (○), the separator/anode interface (◊), and the anode/current collector interface (□) for (a) electrolyte concentration (b) liquid phase potential (c) solid phase potential (d) solid phase surface concentration and (e) solid phase average concentration. The markers represent the finite difference solution, the dashed line for (1,1,1) collocation, the dotted line for the (3,2,3) collocation, and the dash-dotted line for (5,3,5).

The primary advantage of this method is the speed of simulation, which arises because a fewer number of terms are required to obtain a converged solution. Table IX shows the simulation time when using various numbers of collocation points, as well as the root mean squared error (RMSE) relative to the finite difference solution. The times are presented using a FORTRAN based DASSL solver, as well as a Maple[45] solver for all simulations performed. All simulations were run on a computer using a 3.33 GHz Intel processor with 24 GB RAM. Rates of discharge greater than a 1C rate were simulated using

**Table IX. Simulation time and Root Mean Squared Error compared to FD.**

| Method | Number of Differential Algebraic Equations | Simulation Time (Maple) (ms) | Simulation Time (DASSL) (ms) | RSME (mV) |
|---|---|---|---|---|
| Finite Difference (50,35,50) | 590 | N/A[a] | 4617 | – |
| Orthogonal Collocation (1,1,1) | 20 | 781 | 46 | 17.84 |
| Orthogonal Collocation (3,2,3) | 38 | 2355 | 78 | 5.46 |
| Orthogonal Collocation (5,3,5) | 56 | 6022 | 109 | 1.56 |
| Orthogonal Collocation (7,3,7) | 72 | 9812 | 156 | 0.57 |
| 1C Rate MFD (7,3,7) Collocation | 136 | 28361 | 187 | 0.91 |
| 2C Rate MFD (7,3,7) Collocation | 136 | 24680 | 172 | 6.18[b] |
| 5C Rate MFD (9,4,9) Collocation | 170 | 38548 | 234 | 5.29[b] |
| 10C Rate MFD (11,4,11) Collocation | 204 | 64381 | 250 | 9.42[b] |
| 8-Cell Thermal Electrochemical Coupled Stack | 307 | 666608 | 2449 | N/A[c] |

[a] The full order finite difference failed when using Maple solvers.
[b] The 2C, 5C, and 10C rates were compared to a full order MFD finite difference formulation which used 982 equations that took 2106 to 4040 ms to run using DASSL.
[c] An 8-cell thermal electrochemical coupled stack failed when using a full order finite difference.

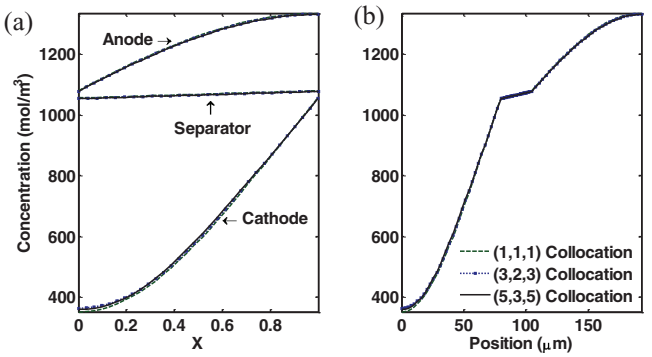


**Figure 5.** Electrolyte concentration across battery for (1,1,1) collocation (dashed line), (3,2,3) collocation (dotted line), and (5,3,5) collocation (solid line) in (a) transformed coordinates and (b) natural coordinates at 3500 seconds of discharge.

the mixed finite difference reformulation for the solid phase concentration in order to accurately track the battery behavior at high rates of discharge. However, the additional number of equations resulting from the mixed finite difference solution results in slower computation, as can be seen in Table IX. Note also that more terms were required to achieve a converged solution when analyzing higher rates.

In order to quantify convergence of the series, the maximum magnitude of the coefficients of successive terms must be analyzed. This is shown in Figure 6, indicating that the first terms are dominant and that the system does converge. Interestingly, the later terms for describing the solid phase concentration carry more weight than for the other variables (although still significantly less than the first term). The behavior of the coefficients for the liquid phase concentration and potential in the separator are nearly completely determined by the constant term alone. In fact, the weight of this term is in excess of 99.99%. This can be explained by analyzing the governing equations for the separator, as given in Table I:

$$\varepsilon_s \frac{\partial c}{\partial t} = \frac{\partial}{\partial x}\left[D_{\text{eff},s}\frac{\partial c}{\partial x}\right] \quad [33]$$

$$-\kappa_{\text{eff},s}\frac{\partial \Phi_2}{\partial x} + \frac{2\kappa_{\text{eff},s}RT}{F}(1-t_+)\frac{\partial \ln c}{\partial x} = I \quad [34]$$

If diffusion occurs quickly enough (which would be expected considering the small thickness of the region), the time derivative term in Equation 33 would approach 0. This leads to a linear concentration profile in the separator if the diffusivity is a constant. Therefore, the cosine terms of Equation (5.6) from Table VI would not contribute much to the final approximation. If the concentration is nearly linear and the reciprocal of concentration is nearly constant, the second term of Equation 34 will be nearly constant. Since the liquid phase conductivity, $\kappa_{\text{eff},s}$, is only a weak function of concentration, and the concentration does not vary appreciably across the separator (see Figure 5), the conductivity will also remain nearly constant. This would lead to a linear profile for the liquid phase potential across the separator. This allows very good accuracy to be retained, even if no cosine terms are used in the separator.

A similar pattern emerges for the solid phase potential in the positive and negative electrodes, with the coefficient of the constant term dominating the cosine terms with a weight of over 99.99%. This suggests that the solid phase potential could be approximated accurately with only the constant term, further reducing the computation required and improving computational speed. However, implementation of this requires that the procedure used be adjusted, as it is required that the collocation points be identical for each variable in the current form. Preliminary attempts to limit the number of terms for the solid phase potential while maintaining a greater number of terms for the remaining variables have been unsuccessful. In our opinion, this is due to the

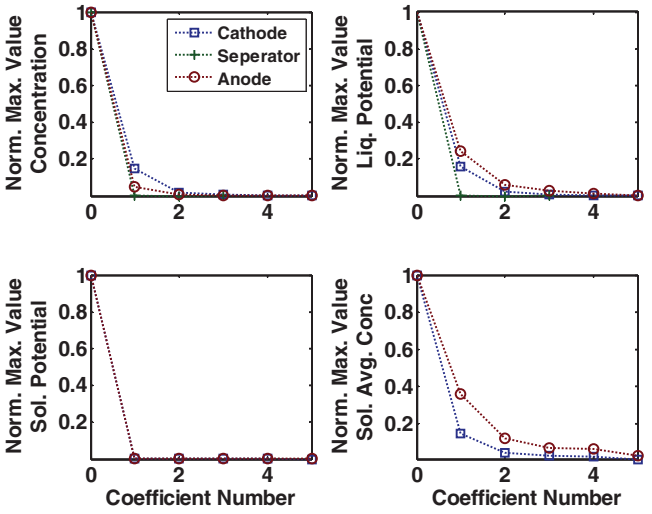


**Figure 6.** Maximum magnitude of coefficients for equations in Table V normalized to the first coefficient term used for (5,3,5) collocation.

fact that although $\Phi_1$ has a nearly flat profile, its spatial derivatives (and therefore current density) have a significant profile across the electrode.

The proposed approach has been used to estimate the values of internal parameters from experimental discharge curves. Also, this approach can simulate continuous battery cycling operation which undergoes constant current/power discharging followed by constant current charging and constant potential charging. This demonstrates the versatility of this method to simulate a wide variety of operating conditions. Figure 7 shows two such cycles which are subject to a constant power discharge of 120 W/m$^2$ a constant current charge of 25 A/m$^2$, followed by a constant current charge at 4.1 V. For comparison, a 1C rate corresponds to ~30 A/m$^2$ using this chemistry. Note that the current state of the internal variables within the battery is carried over from the end of each cycle to the next cycle. Because the internal variables change with time, the behavior of the battery during these cycles is not necessarily identical, perhaps due to incomplete charging of the battery. Also, the internal parameters, such as porosity, etc. can be made to change with cycle number. Therefore, as developments continue in the understanding of capacity fade this continuous cycling procedure can predict the future behavior of the

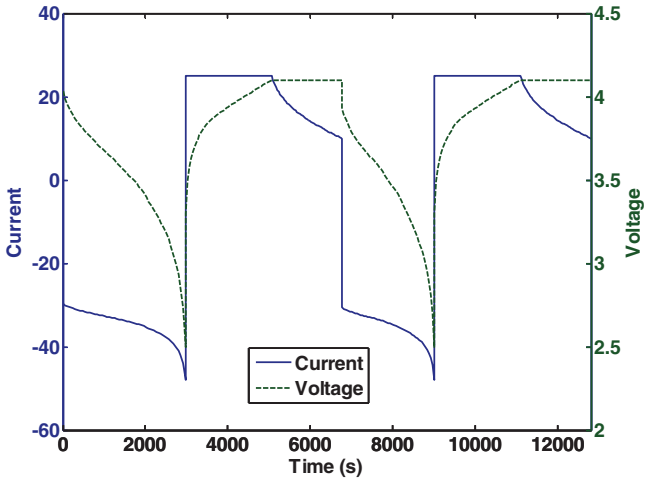


**Figure 7.** Voltage-Time and Current-Time curves for two continuous cycles consisting of constant power discharge followed by constant current charge and constant potential charge.

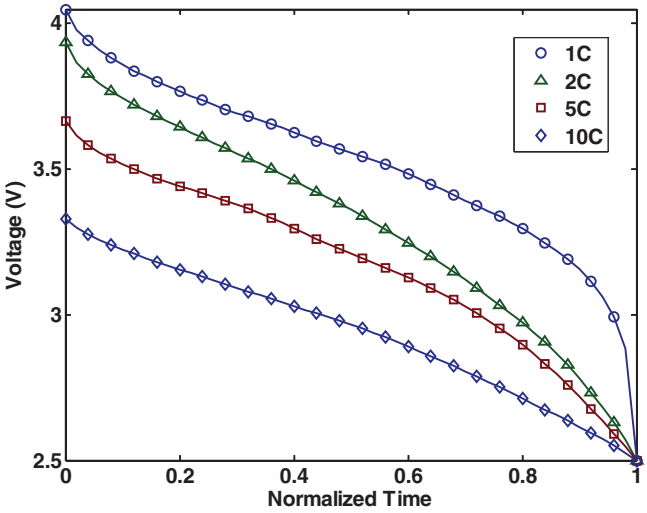


**Figure 8.** Discharge Curve for Higher Discharge Rates.

battery by either changing the parameters already included, or by introducing additional parameters/mechanisms specifically to address capacity fade. This may be achieved by modifying the continuum model directly, or by coupling the continuum model with microscopic models, such as Kinetic Monte Carlo[46–50] or Stress-Strain models[51–53] to create a true multiscale model.

This method can also be used when higher rates of discharge are applied. However, in those circumstances, it is necessary to use the mixed finite difference approximation for the solid phase concentration,[25] rather than the parabolic profile used in the majority of this paper while describing a 1C discharge. The basic method presented for reformulation in the *x*-direction, however, is valid for both parabolic profile approximation and for the mixed finite difference approach. The normalized discharge curve is given in Figure 8 for 1C, 2C, 5C, and 10C rates of discharge, with mixed-finite difference reformulation for solid-phase concentration. Table IX shows the computation time required to simulate the higher discharge conditions, as well as the RMSE of the voltage-time curve relative to a full finite difference. Also, more node points were required to accurately simulate a higher rate discharge when using collocation. It is expected that further improvements in computation time could be achieved by optimizing the initial and maximum time steps in the solver.

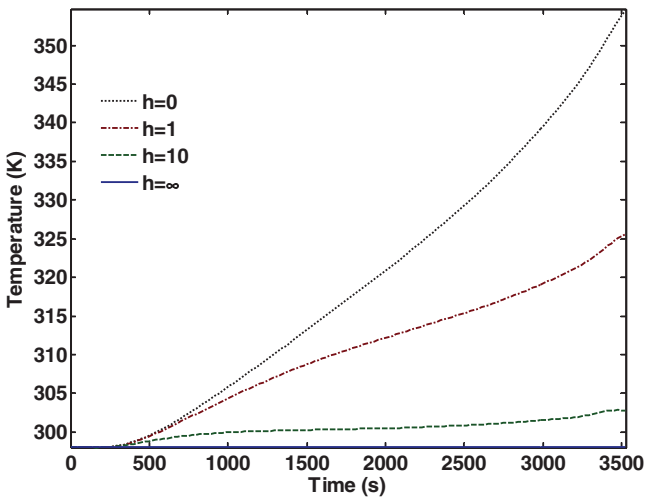


**Figure 9.** Temperature at the center of an 8-cell stack during a 1C rate of discharge subject to varying external heat transfer coefficients.

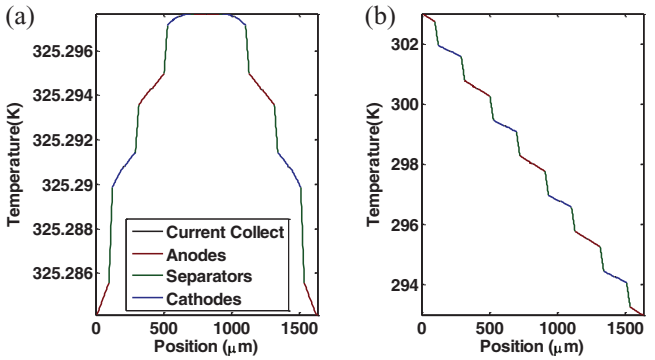


**Figure 10.** Temperature profile across an 8-cell lithium ion battery at the end of discharge when the ends (a) are maintained to be a fixed temperature difference of 10 K and (b) are exposed to a heat transfer coefficient of 1 W/m$^2$K and an ambient temperature of 298 K.

Expanding the model to include the effects of temperature in a multiple cell stack can allow for more detailed simulation, albeit at an increased computational cost (See Table IX). Figure 9 shows the temperature rise at the center of the battery with varying values of the heat transfer coefficients at the end of the stack. For the insulated ($h = 0$) case, there is a 55 K temperature rise within the battery, whereas there in no discernible temperature rise when the battery ends are held at fixed temperature ($h = \infty$). In this case, the battery is sufficiently thin (on the order of microns) that there is not a significant temperature profile within the battery. Figure 10a shows the temperature profile of an 8-cell stack when a heat transfer coefficient of 1 W/m$^2$K is applied to the ends. Notice that the observed variation in the battery is a small fraction of a degree. However, for large batteries, or in two and three dimensions, the possibility of creating a hotspot becomes more significant.

Figure 10b shows the temperature profile within an 8-cell stack when a temperature difference is applied at the ends. The discharge current for the first and last cell in an 8-cell series stack under these conditions is shown in Figure 11. Notice that the current provided by the individual cells are not identical throughout discharge. In this simulation, the temperature of each end of the multi-cell stack is fixed to create temperature decrease of 10 K across the battery. This causes the individual cells to behave differently, resulting in the subtly

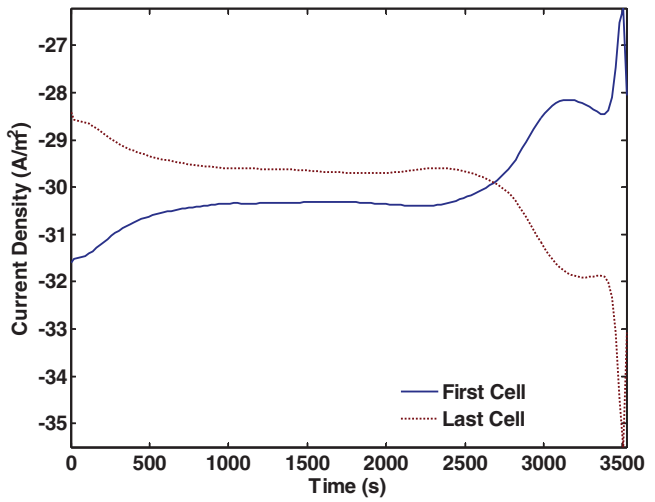


**Figure 11.** Current-Time curves for the first cell (solid line) and last cell (dotted line) within an 8-cell stack with an applied temperature gradient undergoing constant current discharge (1C) using the coupled thermal electrochemical model.

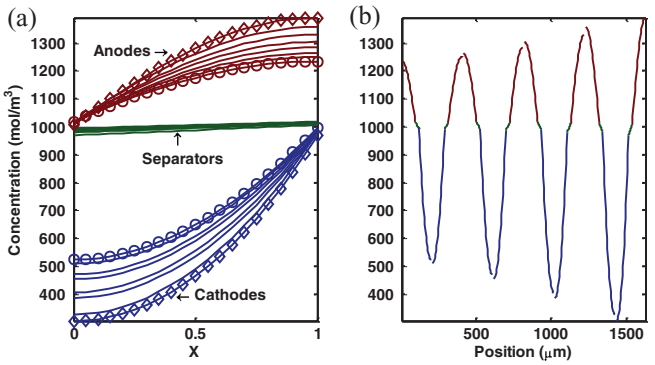


**Figure 12.** Concentration profile across an 8-cell stack at the end of discharge for (a) transformed coordinates and (b) natural coordinates. In (a), (○) denotes the first cell and (◊) denotes the last cell in the series.

different current curves observed in Figure 11. The higher temperature of the first cell causes it to initially discharge at a faster rate than the last cell. However, by the end of discharge, the cooler cell provides a greater current because it exists at a greater state of charge. Figure 12a shows the concentration profile across the entire battery in the transformed coordinates for each individual cell, which further demonstrates how temperature can affect internal battery characteristics. Figure 12b shows the concentration profile across the entire stack in natural coordinates at the end of discharge. Note that there is no electrolyte in the region of the current collectors, leading to a discontinuity at those points. In this example, the stack is sufficiently small that internal heat generation effects do not significantly alter the temperature profile when the ends are held at a fixed temperature. However, for larger stacks, higher applied current and/or different boundary conditions, the temperature profile may be significantly affected by internal heat generation leading to greater behavior variations among the individual cells without an arbitrarily forced condition. The other spatial directions, $y$ and $z$, are important for thermal models at high rates, and the coordinate transformation and the orthogonal collocation approach is still valid. A detailed pseudo 4D model ($x$, $y$, $z$ and $r$) in stack environment can be reduced to a unit cell of $X$, $Y$, $Z$ varying from 0 to 1 in dimensionless transformed coordinates as explained earlier. The proposed approach is also useful for developing models for optimization of graded electrodes or materials wherein control vector parameterization converts a given single region to $N$ regions to represent discrete functions of porosity, particle size or shape.[54–56]

## Conclusion

A coordinate transformation and reformulation of the porous electrode pseudo 2-D model for lithium-ion battery stacks was developed and presented that could be solved accurately and quickly. The coordinate transformation was used to rescale the three regions of the battery model into a single region evaluated on the interval zero to one. This allows collocation to be applied using the zeros of the Jacobi polynomials. This leads to the ability to analytically solve for certain variables prior to using any numerical solver. This results in a system of fewer DAEs which allows for easier (and quicker) computation compared to the traditional finite difference approach.

The reformulation presented is robust enough to be used for a variety of conditions with limited assumptions to maintain the most accurate physics of the model. Although only a single battery chemistry is shown here, this method has been used successfully for a number of different chemistries across a wide range of transport and kinetic parameters. This model thus allows an efficient battery model simulation for use in control and optimization routines, as well as for parameter estimation. Efficient simulation is essential for optimization and parameter estimation because of the large number of simulations that must be run to converge to an appropriate solution. Future work will focus on refining the stack model to allow for simulation of larger stacks, while accounting for multi-scale effects and capacity fade. Additionally, this model will be used in conjunction with optimization routines for lithium-ion battery electrode design to improve performance. The addition of Arrhenius type dependence of diffusion coefficients and reaction rate constants on temperature was also included. This increases the fidelity of the model at the expense of increased complexity and computation time. This approach is robust enough to solve these equations faster than if a finite difference approach were used. This is especially pronounced when a coupled thermal electrochemical multi-cell stack model is used due to the large number of equations that must be solved. However, such a stack model better describes how individual cells operate in the context of a full battery stack. This is important when thermal or other effects cause the individual cells to operate differently from each other. Since it is often not practical or possible to measure each cell individually in a stack, these differences can lead to potentially dangerous or damaging conditions such as overcharging or deep-discharging certain cells within the battery causing thermal runaway or explosions. The ability to efficiently simulate battery stacks facilitates monitoring of individual cell behavior during charging and discharging operations and thereby reducing the chances of temperature buildup causing thermal runaway making the use of stacks safer.

## Acknowledgments

The authors are thankful for the partial financial support of this work by the National Science Foundation under contract number CBET-0828002 and CBET-1008692, International Center for Advanced Renewable Energy and Sustainability at Washington University in St. Louis (I-CARES) and the U.S. government.

## List of Variables

| | |
|---|---|
| $A(t)$ | Coefficient of linear or quadratic term—Solved in terms of B(t) using BCs |
| $a$ | Surface area per volume of electrode |
| $B(t)$ | Collocation coefficients |
| $c$ | Electrolyte concentration |
| $c^s$ | Solid Phase Concentration |
| $D$ | Liquid phase Diffusion coefficient |
| $D_{eff}$ | Effective Diffusion coefficient |
| $D^s$ | Solid phase diffusion coefficient |
| $E_a$ | Activation Energy |
| $F$ | Faraday's Constant |
| $h$ | Heat Transfer Coefficient |
| $I$ | Applied Current |
| $j$ | Pore wall flux |
| $k$ | Reaction rate constant |
| $l$ | Length of region |
| $N$ | Number of terms to approximate the solution |
| $P(x)$ | Jacobi Polynomial |
| $R$ | Particle Radius, or Residual |
| $t_+$ | Transference number |
| $T$ | Temperature |
| $U$ | Open Circuit Potential |
| $W$ | Weight Function |
| $\alpha, \beta$ | Characteristics of the Jacobi polynomial |
| $\varepsilon$ | Porosity |
| $\varepsilon_f$ | Filling fraction |
| $\theta$ | State of Charge |
| $\kappa$ | Liquid phase conductivity |
| $\sigma$ | Solid Phase Conductivity |
| $\Phi_1$ | Solid Phase Potential |
| $\Phi_2$ | Liquid Phase Potential |

## List of Subscripts

| | |
|---|---|
| *eff* | Effective, as for diffusivity or conductivity |
| *c* | Related to Electrolyte concentration |
| $c^s$ | Related to Solid Phase concentration |
| *n* | Related to the negative electrode—the anode |
| *p* | Related to the positive electrode—the cathode |
| *s* | Related to the separator |
| $\Phi_1$ | Related to the solid phase potential |
| $\Phi_2$ | Related to the liquid phase potential |

## List of Superscripts

| | |
|---|---|
| *avg* | Average, as for solid phase concentration |
| *surf* | Surface, as for solid phase concentration |
| *s* | Related to Solid Phase |

## References


1. M. Doyle, T. F. Fuller, and J. Newman, *J. Electrochem. Soc.*, **140**, 1526 (1993).
2. J. Newman and W. Tiedemann, *AIChE J.*, **21**, 25 (1975).
3. T. F. Fuller, M. Doyle, and J. Newman, *J. Electrochem. Soc.*, **141**, 982 (1994).
4. T. F. Fuller, M. Doyle, and J. Newman, *J. Electrochem. Soc.*, **141**, 1 (1994).
5. M. Doyle, J. Newman, A. S. Gozdz, C. N. Schmutz, and J. M. Tarascon, *J. Electrochem. Soc.*, **143**, 1890 (1996).
6. K. E. Thomas and J. Newman, *J. Electrochem. Soc.*, **150**, A176 (2003).
7. P. Arora, M. Doyle, A. S. Gozdz, R. E. White, and J. Newman, *J. Power Sources*, **88**, 219 (2000).
8. P. Ramadass, B. Haran, R. E. White, and B. N. Popov, *J. Power Sources*, **123**, 230 (2003).
9. P. Ramadass, B. Haran, P. M. Gomadam, R. E. White, and B. N. Popov, *J. Electrochem. Soc.*, **151**, A196 (2004).
10. G. Ning, R. E. White, and B. N. Popov, *Electrochim. Acta*, **51**, 2012 (2006).
11. G. G. Botte, V. R. Subramanian, and R. E. White, *Electrochim. Acta*, **45**, 2595 (2000).
12. P. M. Gomadam, J. W. Weidner, R. A. Dougal, and R. E. White, *J. Power Sources*, **110**, 267 (2002).
13. S. Santhanagopalan, Q. Guo, P. Ramadass, and R. E. White, *J. Power Sources*, **156**, 620 (2006).
14. V. R. Subramanian, V. D. Diwakar, and D. Tapriyal, *J. Electrochem. Soc.*, **152**, A2002 (2005).
15. C. Y. Wang, W. B. Gu, and B. Y. Liaw, *J. Electrochem. Soc.*, **145**, 3407 (1998).
16. K. Smith and C. Y. Wang, *J. Power Sources*, **161**, 628 (2006).
17. V. Balakotaiah and S. Chakraborty, *Chem. Eng. Sci.*, **58**, 4769 (2003).
18. V. Balakotaiah and H.-C. Chang, *SIAM J. Appl. Math.*, **63**, 1231 (2003).
19. F. A. Howes and S. Whitaker, *Chem. Eng. Sci.*, **40**, 1387 (1985).
20. M. Golubitky and D. G. Schaeffer, *Singularities and Groups in Bifurcation Theory*, Vol. 1, Springer-Verlag, Berlin (1984).
21. Q. Zhang and R. E. White, *J. Power Sources*, **165**, 880 (2007).
22. V. R. Subramanian, V. D. Diwakar, and D. Tapriyal, *J. Electrochem. Soc.*, **152**, A2002 (2005).
23. S. Liu, *Solid State Ionics*, **177**, 53 (2006).
24. K. Smith and C. Y. Wang, *J. Power Sources*, **161**, 628 (2006).
25. V. Ramadesigan, V. Boovaragavan, J. Carl Pirkle, Jr., and V. R. Subramanian, *J. Electrochem. Soc.*, **157**, A854 (2010).
26. K. E. Brenan, S. L. Campbell, and L. R. Petzold, *Numerical Solution of Initial-Value Problems in Differential-Algebraic Equations*, North-Holland, New York (1989).
27. L. Cai and R. E. White, *J. Electrochem. Soc.*, **156**, A154 (2009).
28. V. R. Subramanian, V. Boovaragavan, V. Ramadesigan, and M. Arabandi, *J. Electrochem. Soc.*, **156**, A260 (2009).
29. L. Cai and R. E. White, Paper 1126, *presented at the Electrochemical Society Meeting*, Las Vegas, NV, October 10–15, 2010.
30. S. Lee, Y. Kim, and H. Chun, *Electrochimica Acta.*, **47**, 1055 (2002).
31. J. C. Forman, S. Bashash, J. L. Stein, and H. K. Fathy, *J. Electrochem. Soc.*, **158**, A193 (2011).
32. G. F. Carey and B. A. Finlayson, *Chem. Eng. Sci.*, **30**, 587 (1975).
33. J. Villadsen and M. L. Michelsen, *Solution of Differental Equation Models by Polynomial Approximation*, p. 111, Prentice-Hall, Inc., Englewood Cliffs, NJ (1978).
34. D. Bernardi, E. Pawlikowski, and J. Newman, *J. Electrochem. Soc.*, **132**, 5 (1985).
35. C. R. Pals and J. Newman, *J. Electrochem. Soc.*, **142**, 3274 (1995).
36. L. Rao and J. Newman, *J. Electrochem. Soc.*, **144**, 2697 (1997).
37. L. Song and J. W. Evans, *J. Electrochem. Soc.*, **147**, 2086 (2000).
38. W. B. Gu and C. Y. Wang, *J. Electrochem. Soc.*, **147**, 2910 (2000).
39. K. Kumaresan, G. Sikha, and R. E. White, *J. Electrochem. Soc.*, **155**, A164 (2000).
40. C. R. Pals and J. Newman, *J. Electrochem. Soc.*, **142**, 3282 (1995).
41. Y. Chen and J. W. Evans, *J. Electrochem. Soc.*, **141**, 2947 (1994).
42. Y. Chen and J. W. Evans, *J. Electrochem. Soc.*, **143**, 2708 (1996).
43. L. O. Valøen and J. N. Reimers, *J. Electrochem. Soc.*, **152**, A882 (2005).
44. M. Guo, G. Sikha, and R. E. White, *J. Electrochem. Soc.*, **158**, A122 (2011).
45. http://www.maplesoft.com/Products/Maple, last accessed: May 20, 2011.
46. J. Bhattacharya and A. Van der Ven, *Physical Review B*, **81**, 104304 (2010).
47. A. B. Bortz, M. H. Kalos, and L. Lebowitz, *J. Comput. Phys*, **17**, 10 (1975).
48. A. Van der Ven and G. Cedar, *Electrochemical & Solid-State Letters*, **3**(7), 301 (2000).
49. T. O. Drews, R. D. Braatz, and R. C. Alkire, *Z. Phys. Chem.*, **221**, 1 (2007).
50. R. N. Methekar, P. W. C. Northrop, K. Chen, R. D. Braatz, and V. R. Subramanian, *J. Electrochem. Soc.*, **158**, A363 (2011).
51. J. Christensen and J. Newman, *J. Electrochem. Soc.*, **153**, A1019 (2006).
52. X. Zhang, W. Shyy, and A. M. Sastry, *J. Electrochem. Soc.*, **154**, A910 (2007).
53. S. Renganathan, G. Sikha, S. Santhanagopalan, and R. E. White, *J. Electrochem. Soc.*, **157**, A155 (2010).
54. V. Ramadesigan, R. N. Methekar, F. Latino, R. D. Braatz, and V. R. Subramanian, *J. Electrochem. Soc.*, **157**, A1328 (2010).
55. S. Kameswaran and L. T. Biegler, *Comput. Chem. Eng.*, **30**, 1560 (2006).
56. M. Schlegel, K. Stockmann, T. Binder, and W. Marquardt, *Comput. Chem. Eng.*, **29**, 1731 (2005).